Cell

Local hyperthermia therapy induces browning of white fat and treats obesity

Graphical abstract

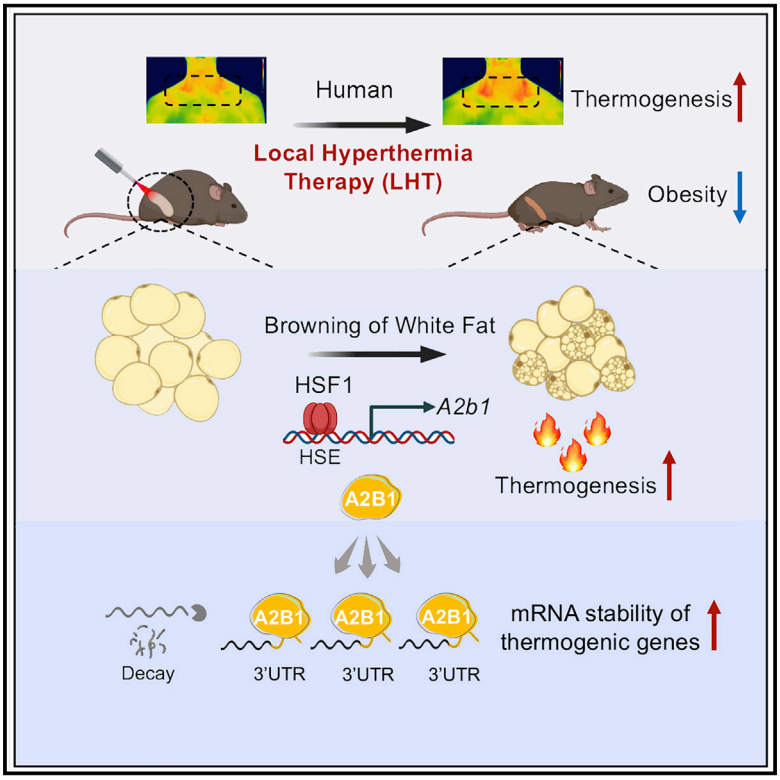

Highlights

- Local hyperthermia therapy (LHT) induces thermogenesis in mouse and human adipocytes
- HSF1 is indispensable for the effects of chronic LHT against obesity in mice
- HNRNPA2B1 acts downstream of HSF1 to enhance stability of metabolic gene transcripts
- A human HSF1 variant improves HNRNPA2B1 expression and measures of beige fat function

Authors

Yu Li, Dongmei Wang, Xiaodan Ping, ..., Cheng Hu, Lingyan Xu, Xinran Ma

Correspondence

qzhang@bio.ecnu.edu.cn (Q.Z.), alfredhc@sjtu.edu.cn (C.H.), lyxu@bio.ecnu.edu.cn (L.X.), xrma@bio.ecnu.edu.cn (X.M.)

In brief

Local application of heat leads to the activation of beige fat in mice and humans, suggesting a novel approach to counter obesity.

Li et al., 2022, Cell *185*, 949–966
March 17, 2022
https://doi.org/10.1016/j.cell.2022.02.004

CellPress

Cell

CellPress

Article

Local hyperthermia therapy induces browning of white fat and treats obesity

Yu Li,[1,6] Dongmei Wang,[1,6] Xiaodan Ping,[1] Yankang Zhang,[1] Ting Zhang,[1] Li Wang,[1] Li Jin,[2] Wenjun Zhao,[1] Mingwei Guo,[1] Fei Shen,[1] Meiyao Meng,[1] Xin Chen,[1] Ying Zheng,[1] Jiqiu Wang,[4] Dali Li,[1,5] Qiang Zhang,[1,*] Cheng Hu,[2,3,*] Lingyan Xu,[1,5,*] and Xinran Ma[1,3,5,7,*]

[1]Shanghai Key Laboratory of Regulatory Biology, Institute of Biomedical Sciences, School of Life Sciences, East China Normal University, Shanghai 200241, China

[2]Shanghai Diabetes Institute, Shanghai Key Laboratory of Diabetes Mellitus, Shanghai Clinical Centre for Diabetes, Shanghai Jiao Tong University Affiliated Sixth People's Hospital, Shanghai 200233, China

[3]Department of Endocrinology and Metabolism, Fengxian Central Hospital Affiliated to Southern Medical University, Shanghai 201499, China

[4]Department of Endocrinology and Metabolism, Ruijin Hospital, Shanghai Jiao Tong University School of Medicine, Shanghai 200025, China

[5]Shanghai Frontiers Science Center of Genome Editing and Cell Therapy, Shanghai Key Laboratory of Regulatory Biology and School of Life Sciences, East China Normal University, Shanghai 200241, China

[6]These authors contributed equally

[7]Lead contact

*Correspondence: qzhang@bio.ecnu.edu.cn (Q.Z.), alfredhc@sjtu.edu.cn (C.H.), lyxu@bio.ecnu.edu.cn (L.X.), xrma@bio.ecnu.edu.cn (X.M.)

https://doi.org/10.1016/j.cell.2022.02.004

SUMMARY

Beige fat plays key roles in the regulation of systemic energy homeostasis; however, detailed mechanisms and safe strategy for its activation remain elusive. In this study, we discovered that local hyperthermia therapy (LHT) targeting beige fat promoted its activation in humans and mice. LHT achieved using a hydrogel-based photothermal therapy activated beige fat, preventing and treating obesity in mice without adverse effects. HSF1 is required for the effects since HSF1 deficiency blunted the metabolic benefits of LHT. HSF1 regulates *Hnrnpa2b1* (*A2b1*) transcription, leading to increased mRNA stability of key metabolic genes. Importantly, analysis of human association studies followed by functional analysis revealed that the HSF1 gain-of-function variant p.P365T is associated with improved metabolic performance in humans and increased *A2b1* transcription in mice and cells. Overall, we demonstrate that LHT offers a promising strategy against obesity by inducing beige fat activation via HSF1-A2B1 transcriptional axis.

INTRODUCTION

Obesity, the excess accumulation of fat in adipose tissues, often entails metabolic derangement and a predisposition to metabolic diseases including type 2 diabetes (T2DM), hepatic steatosis, and cardiovascular diseases (Ji and Guo, 2019). As an endocrine organ of pleiotropic functions, adipose tissues are classified as white, brown, and beige fat based on their anatomic location and metabolic functions (Rosen and Spiegelman, 2014; Scheja and Heeren, 2019). Particularly, beige fat exists in clusters amid white fat and is indistinguishable from white adipocytes under basal state but undergoes a process called browning of white fat when activated, i.e., by cold stimuli or beta-adrenergic signaling, and exhibits strong induction in brown gene programs and heat production (Barbatelli et al., 2010; Harms and Seale, 2013; Wu et al., 2012). Of clinical significance, cold-inducible beige fat is found to exist in adult human around the supraclavicular region and thus offers great therapeutic potential for metabolic diseases (van Marken Lichtenbelt et al., 2009; Nedergaard et al., 2007; Virtanen et al., 2009). Previous studies implemented cold stimuli or adrenergic signaling activation as a useful way to activate beige fat (Harms and Seale, 2013; Vitali et al., 2012). However, these treatments have limited applications because of the various health concerns and potential cardiovascular hazards (Bhadada et al., 2011; Larsen et al., 2002; Redman et al., 2007; Vasconcelos et al., 2013). Thus, facing the obesity epidemic, it is urgent to discover promising gene targets and approaches to achieve safe and effective beige fat activation.

Intriguingly, hyperthermia therapy (HT), which results in temporary hyperthermia through heating methods such as sauna or hot tub bathing, has drawn increasing scientific interests as a therapeutic practice for metabolic diseases (Brunt et al., 2016; Laukkanen et al., 2015). For example, treating T2DM patients with 3 weeks of daily hot tub bathing improved metabolic parameters including decreased HbA1, mild weight loss, and improved diabetic neuropathic symptoms (Hooper, 1999). HT through warm water immersion also conferred metabolic improvements in various animal models (Archer et al., 2018). These data support the notion of implementing hyperthermia as a therapeutic revenue to combat obesity, though many questions remain. For example,

previous studies utilized HT against whole body; thus, it is not clear which tissue plays a major role in mediating the metabolic benefits of the therapy. Moreover, prolonged hot water submersion poses potential neurological and cardiovascular risks (Masuda et al., 2019) caused by increased core body temperature and stress hormones production. Lastly, though the induction of heat shock protein 72 (HSP72) has been implicated as a potential mechanism of the beneficial effects of HT (Chung et al., 2008), detailed mechanistic insights are lacking. It is thus desirable to find innovative ways of locally delivered HT to avoid side effects of whole-body HT and for better mechanistic unraveling. In this regard, beige fat has recently been shown to be able to sense temperature changes in a cell-autonomous and β-adrenergic-receptor-independent way (Ye et al., 2013), rendering it a promising metabolic target of local hyperthermia therapy (LHT).

HSF1 is a transcription factor that orchestrates cellular responses to various stresses, including heat stress, via its regulation on HSPs for protein refolding and homeostasis (Gomez-Pastor et al., 2018) and is critical in various cancers (Dai and Sampson, 2016) as well as longevity (Baird et al., 2014). Recent studies utilizing sequencing analysis indicated that HSF1 might regulate a broader array of target genes beyond the scope of chaperones in cancer (Dong et al., 2019; Mendillo et al., 2012). Notably, we and others have identified a molecular link between HSF1 and PGC1α, a master regulator of energy homeostasis, in multiple tissues (Gomez-Pastor et al., 2017; Ma et al., 2015; Qiao et al., 2017; Xu et al., 2016). These studies indicated that HSF1 may exert vital functions aside from its classic role in protein refolding. Thus, in this study, we comprehensively investigated the role of LHT in thermogenesis and fat metabolism and deciphered its mechanisms via HSF1 activation, which would provide therapeutic strategies against obesity and metabolic diseases.

RESULTS

Hyperthermia induces thermogenesis and brown gene programs *in vitro* and *in vivo*

To test whether beige adipocytes could sense hyperthermia in a cell-autonomous way, we subjected beige adipocytes to hyperthermia environment (HT, 41°C) or control (Con, 37°C) treatment. Both samples were then maintained in regular culture environments (37°C) and examined to see the impacts of hyperthermia. We found that HT of various lengths of time all induced the expression of *Ucp1*, a key protein in thermogenesis, to different extents (Figure S1A). We chose 2-h HT in next *in vitro* studies for its highest *Ucp1* induction. We assessed the effect of HT on thermogenesis using a small molecule thermosensitive fluorescent dye, ERthermAC, which is capable of monitoring temperature rising in thermogenic adipocytes (Kriszt et al., 2017; Nguyen et al., 2020). Intriguingly, compared with control, ERthermAC fluorescent intensity was significantly decreased after HT to a similar extent under the positive control forskolin (FSK) or CL316,243 (CL) treatment, indicating higher temperature and enhanced thermogenesis in beige adipocytes (Figure 1A). Importantly, we found that the expression of thermogenic gene programs including *Pgc1α* and *Ucp1*, the markers for mitochondrial biogenesis and thermogenesis, featured significant increases in HT cells (Figure 1B), while the viability of beige adipocytes was not affected by HT (Figure S1B). In addition, HT cells were cultured in regular temperature at 37°C incubator before subjecting to various assays, thus eliminating any potential effects of hyperthermia itself on cellular temperature.

We next investigated whether LHT could activate beige fat thermogenesis *in vivo*. Polyethylene glycol (PEG)-crosslinked polydopamine nanoparticle (PDA), a biosafe and injectable photothermal hydrogel, is capable of converting near-infrared (NIR) light input into accurately controlled temperature output (Cheng et al., 2019; Liu et al., 2014; Wang et al., 2016b; Zhou et al., 2017). We injected mice with PEG-PDA hydrogel (termed PDA) subcutaneously in bilateral inguinal white adipose tissues (iWATs), then illuminated one side of iWATs with non-invasive, non-harmful NIR laser to achieve homogeneous hyperthermia in iWAT (LHT) at 41°C ± 0.5°C for 10 min, while the other side underwent the same sham manipulation without NIR laser illumination (Sham) (Figure 1C). Critically, skin temperatures were elevated during LHT, while no obvious change in core body temperatures were observed during the whole process (Figure S1C).

Strikingly, compared with pretreatment, LHT on iWAT resulted in significantly enhanced heat production in iWAT compared with Sham iWAT of the same mouse (Figure 1D). Molecular analysis in iWAT showed increased mRNA levels of brown gene programs, as well as increased UCP1 protein levels in LHT group (Figures 1E and 1F). The higher temperature in LHT iWAT is irrelevant to hyperthermia itself, since mice were removed from NIR illumination before any assay was performed. Intriguingly, brown adipose tissue (BAT) is less sensitive to LHT, as LHT on BAT resulted in dampened responses (Figure S1D). In order to rule out the possibility that LHT exhibited effects via macrophages, which have been reported to be involved in beige adipocytes activation and thermogenesis (Chen et al., 2021; Henriques et al., 2020; Nguyen et al., 2011), we depleted macrophages in iWAT and still observed sustained increase in *Ucp1* expression after LHT in mice, suggesting that LHT-induced beige fat thermogenesis was independent of macrophages (Figure S1E). Besides, LHT in iWAT did not lead to significant changes in angiogenic or sympathetic neuron growth gene programs, which were reported to impact thermogenesis (Pellegrinelli et al., 2018; Seki et al., 2018; Zeng et al., 2019) (Figures S1F and S1G). Notably, we found that LHT increased blood flow in iWAT, but not in BAT, while norepinephrine (NE) levels in serum and in iWAT, NE turnover rate in iWAT, cortisol levels in serum, and thermogenic and mitochondrial gene programs in BAT were not changed in mice after LHT on iWAT (Figures S1H–S1K), overall demonstrating that unlike whole-body HT, LHT in iWAT caused no overt changes in stress hormone production systemically or locally and thus ruled out the possibility that the increased thermogenesis was due to sympathetic activation upon heat stress. Taken together, these *in vitro* and *in vivo* data suggested that LHT promoted thermogenesis and brown gene programs in beige adipocytes in a cell-autonomous fashion.

Adult humans have been demonstrated to possess beige fat mainly in the supraclavicular region (Jespersen et al., 2013; Wu et al., 2012). Therefore, we then set out to examine the human relevance of the impact of LHT on beige fat thermogenesis. Adult male and female volunteers were set in a temperature- and humidity-controlled environment. After 60-min acclimation (van

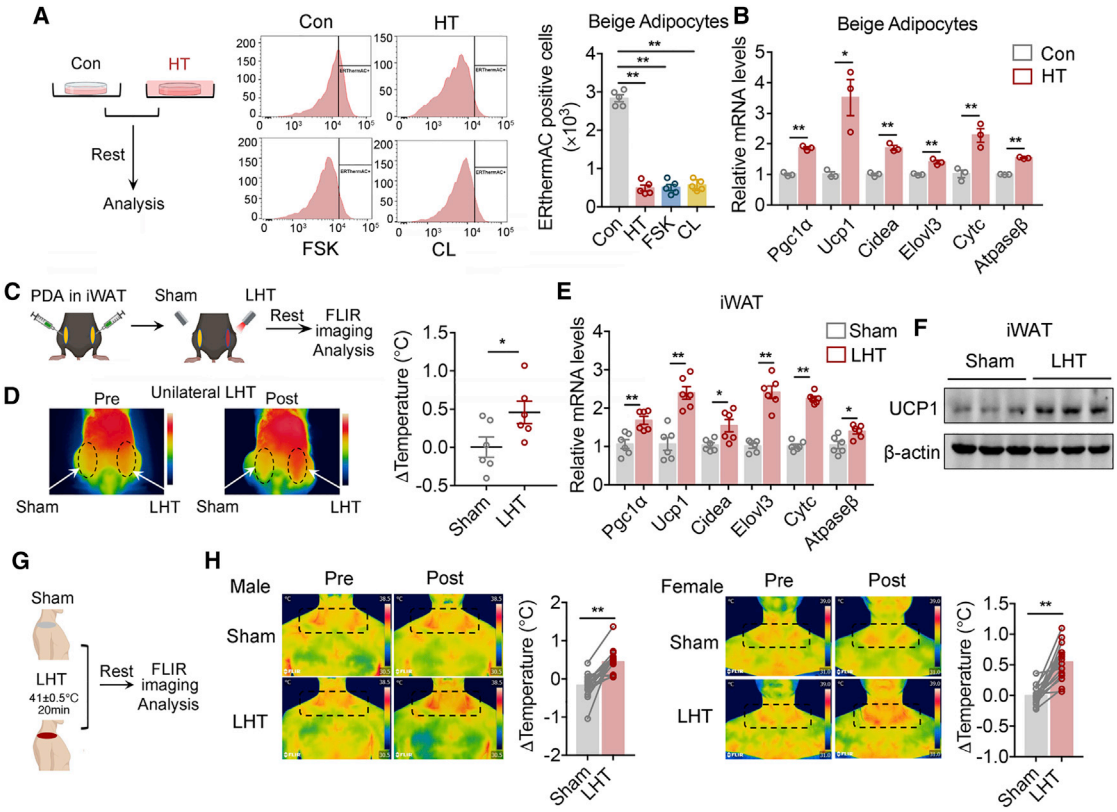

Figure 1. Hyperthermia therapy induces thermogenesis and brown gene programs both *in vitro* and *in vivo*

(A) Flow cytometry analysis of the thermosensitive fluorescent dye stained ERthermAC-positive cells in C3H10T1/2-derived beige adipocytes treated with 37°C (Con) or 41°C hyperthermia therapy (HT) and rested for 12 h at 37°C, with forskolin (FSK) and β3-adrenergic receptor agonist CL316,243 (CL) as the positive control (n = 5).

(B) mRNA levels of thermogenic and mitochondrial genes in control or HT-treated immortalized beige adipocytes (n = 3).

(C) Schematic representation of mice inguinal fat injected with PDA and underwent unilateral non-invasive, non-harmful NIR laser exposure as local hyperthermia therapy (LHT) at 41°C ± 0.5°C or with Sham procedure for 10 min and rested for 24 h.

(D) Representative thermal images as shown by FLIR image (left) and quantification of temperature changes (ΔTemperature, post-pre) (right) under Sham or LHT in iWAT. (n = 6).

(E and F) mRNA levels of thermogenic and mitochondrial genes (E), as well as immunoblotting for UCP1 protein levels (F) in unilateral iWAT under Sham or LHT (n = 6).

(G) Schematic representation of thermal imaging of human supraclavicular area pre or post to Sham or 20 min LHT at 41°C ± 0.5°C and rest for 2 h.

(H) Representative thermal images as shown by the FLIR image (left) and quantification of the temperature change of supraclavicular area (ΔTemperature, post-pre) (right) in humans under Sham or LHT (male n = 17, female n = 16).

Statistical significance was assessed by unpaired Student's t test (A, B, D, and E) or paired Student's t test (H). Data are presented as mean ± SEM and *p < 0.05 and **p < 0.01.

See also Figure S1.

Marken Lichtenbelt et al., 2009; Bakker et al., 2014), a thermal source of 41°C ± 0.5°C was applied locally to the supraclavicular fat depots of each subject for 20 min (Figure 1G). The core temperatures of all volunteers remained unperturbed along the test process (Figure S1L). The thermal signatures of individuals were visualized with FLIR system before LHT and recorded again after removal of heat source and a rest period to avoid the influence of hyperthermia itself on temperatures (Figure 1G). Afterward, the exact same experimental protocols were repeated but without thermal source application on each volunteer as Sham. As representative FLIR images shown in Figure 1H, compared with pretreatment, LHT significantly enhanced heat production in the supraclavicular depot around the neck area compared with Sham, without affecting serum NE levels (Figure S1M). These results signified that LHT could also induce thermogenesis in human, possibly by the activation of beige adipocytes, without elevating core body temperature or catecholamine signaling. Of note, the effects of LHT were still present after 5-week long-term treatment, suggesting prolonged effectiveness of LHT in humans (Figure S1N).

Chronic LHT protected and treated obesity in mice

Considering the acute effects of LHT on beige fat thermogenesis in mice and in humans, it is worthwhile to study the long-term impact of chronic LHT on metabolic performances. First, to eliminate any toxic effects, we examined whether PDA would cause

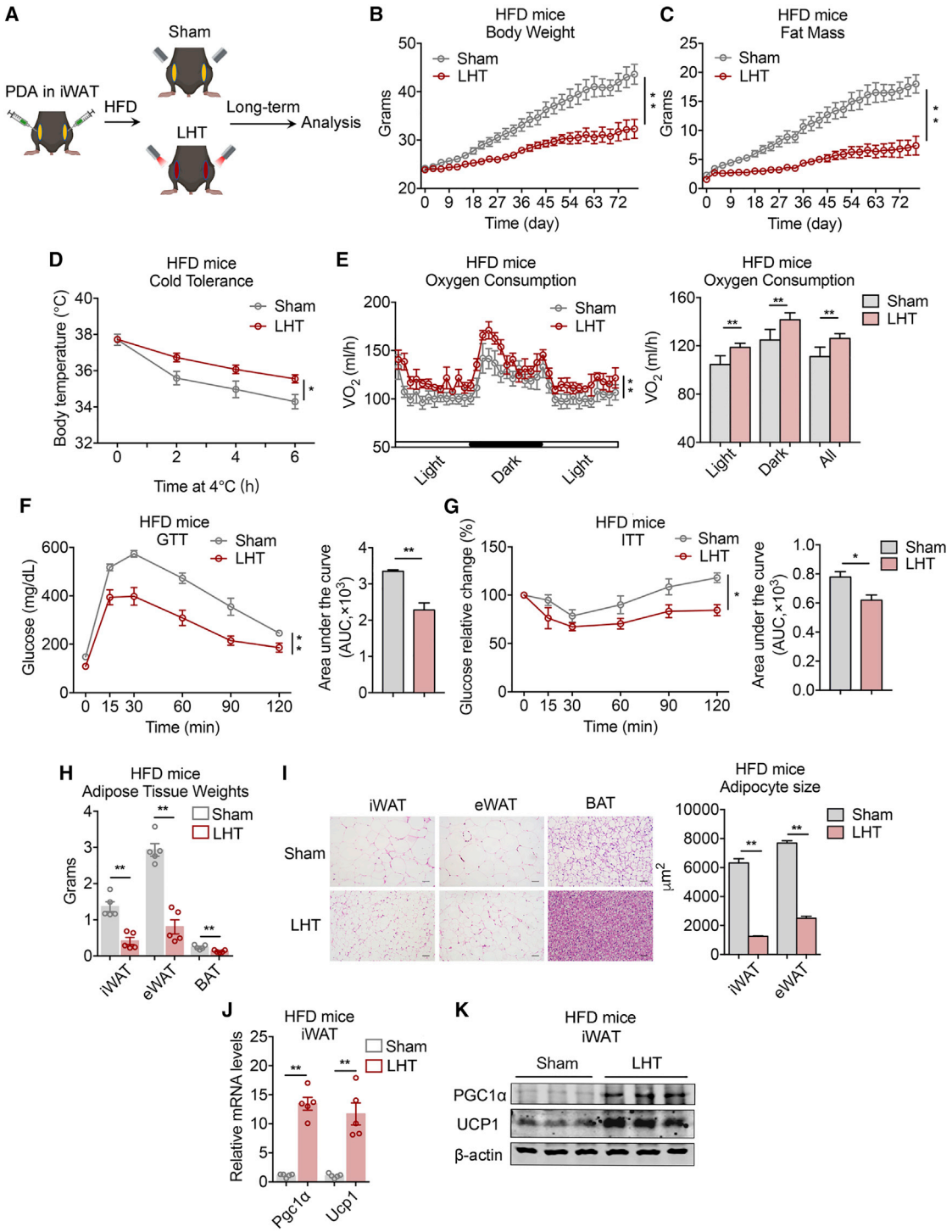

Figure 2. Chronic local hyperthermia therapy protected from diet-induced obesity in mice

(A) Schematic figure of chronic local hyperthermia therapy: mice under high-fat diet (HFD) were injected with PDA in bilateral iWATs and treated without NIR illumination (Sham) or with NIR laser (LHT) for 10 min on each side of iWAT once every 3 days for over 10 weeks.

(B–K) Analysis of metabolic performances of mice treated chronically with Sham or LHT (n = 5) as described in (A), including (B) body weight, (C) fat mass, (D) cold tolerance, (E) whole-body oxygen consumption, (F) GTT, (G) insulin tolerance test (ITT), (H) adipose tissue weights, (I) representative H&E staining of adipose tissues, (J) mRNA levels of *Pgc1α* and *Ucp1* genes in iWAT, and (K) immunoblotting for PGC1α and UCP1 protein levels in iWAT.

(legend continued on next page)

any long-term defect in mice injected with PDA or PBS subcutaneously in bilateral iWATs and subjected to a high-fat diet (HFD) (Figure S2A). We found that PDA group showed similar body weight accretion compared with PBS group (Figure S2B). Subsequent thorough comparison of organ weights, tissue morphology, and serum parameters including liver and kidney function analysis between PDA and PBS groups revealed no obvious toxicity of PDA in mice (Figures S2C–S2E; Table S1).

We then set out to test the metabolic effects of long-term LHT in mice. Bilateral LHT models were established whereas mice were injected with PDA in bilateral iWATs and subjected to HFD. They were then treated with NIR laser (HFD LHT) or Sham treated without NIR illumination (HFD Sham) once every 3 days for over 10 weeks (Figure 2A). Strikingly, HFD LHT mice showed significantly reduced body weights mainly contributed by a reduction in fat mass (Figures 2B and 2C), accompanied with enhanced cold tolerance capability (Figure 2D) and elevated energy expenditure (Figure 2E). HFD LHT group also showed better metabolic fitness, i.e., improved serum parameters (Figure S2F), enhanced insulin sensitivity (Figures 2F and 2G) compared with HFD Sham, while NE levels in serum and iWAT, food intake, and locomotor activity were similar between the two groups (Figures S2G–S2I). Detailed tissue analysis revealed that HFD LHT mice have significantly smaller adipose depots and largely ameliorated hepatic steatosis, with consistently smaller adipocyte sizes and less lipid accumulation in livers under histological examination (Figures 2H, 2I, and S2J). Chronic LHT caused no adverse effect, as demonstrated by similar serum liver and kidney function parameters, as well as comparable major organ weights between HFD LHT and Sham mice (Figure S2K; Table S1). At the molecular level, we found increased expression of Pgc1α and Ucp1 in both mRNA and protein levels (Figures 2J and 2K). Of note, we observed enhanced energy expenditure and increased brown gene programs in iWAT of LHT mice in the first week of treatment (early HFD), prior to significant body weight changes and without differences in food intake (Figures S2L–S2N).

Thinking from a therapeutic standpoint, we applied chronic LHT on diet-induced obese (DIO) mice to study its effects in treating obesity. Mice were first fed HFD to induce a body weight increase to over 40 g, then injected with PDA in bilateral iWATs, and treated with (DIO LHT) or without NIR (DIO Sham) once every 3 days (Figure S3A). Prolonged treatment led to similar metabolic benefits of LHT in DIO LHT mice as in HFD LHT mice, including reduced body weights, fat mass, alleviated adipose tissue weights, improved insulin sensitivity, hepatic steatosis, and serum parameters and increased expression of Pgc1α and Ucp1 in both mRNA and protein levels (Figures S3B–S3K), with no obvious side effects in LHT-treated DIO mice compared with their controls (Table S1). Besides, we observed increased energy expenditure in DIO LHT mice compared with Sham in the first week of treatment (early DIO), without changes in food intake or residual energy in feces (Figures S3L and S3M). Together, these results suggest that chronic LHT can both prevent and treat obesity and metabolic dysfunctions, possibly through the activation of beige fat in mice.

HSF1 is indispensable for the effects of LHT in adipocytes and in mice

Next, we set out to unravel the mechanism of LHT on beige fat activation. HSF1 and transient receptor potential channel, vanilloid subfamily member 1 (TRPV1), are classic heat-responsive proteins critical in orchestrating cellular response to heat, and their functions have also been implicated in fat biology, energy metabolism, and obesity (Baler et al., 1993; Baskaran et al., 2016; Caterina et al., 1997; Gomez-Pastor et al., 2018; Ma et al., 2015; Xu et al., 2016). Therefore, we delivered specific siRNA targeting Hsf1 and Trpv1, respectively, into beige adipocytes to investigate their essentialness in the metabolic responses of beige adipocytes toward LHT. Compared with scramble controls (Scr), TRPV1 knockdown caused no obvious changes possibly due to higher temperature threshold $\sim$43°C for TPRV1 activation (Caterina et al., 1997), while HSF1 deficiency largely blunted LHT-induced Pgc1α and Ucp1 expressions in beige adipocytes (Figure S4A), suggesting that HSF1 might be vital for LHT-induced thermogenesis in adipose tissues.

To further test this hypothesis *in vivo*, we generated HSF1 fat conditional knockout mice (HSF1 FKO) by crossing Adiponectin-Cre mice with HSF1-loxp mice (Figure S4B). Comprehensive characterizations of the metabolic performances of HSF1 FKO mice showed that, under normal chow diet (NCD), wild-type (WT), and HSF1 FKO mice have similar body weights and body mass compositions, comparable fat depot and liver weights, and tissue morphology (Figures S4C–S4E). Interestingly, molecular analysis revealed that HSF1 FKO mice showed impaired thermogenic gene program in iWAT, but not in BAT, indicating that the loss of HSF1 in fat may cause a specific functional defect in iWAT (Figure S4F). This might be due the mild HSF1 activity under basal condition in beige adipocytes, since we found that HSF1 characterized partial nuclear localization associated with higher UCP1 expression in primary beige adipocytes (Figure S4G).

Next, we put WT and HSF1 FKO mice under a HFD challenge, which unveiled that HSF1 FKO mice featured increased adiposity compared with WT, as shown by elevated body weights, fat mass, adipose tissue weights, and adipocyte sizes, as well as more severe insulin resistance and hepatic steatosis (Figures 3A–3F and S4H). Moreover, HSF1 deficiency in fat resulted in impaired thermogenic capability in mice, as shown by decreased core temperature during cold challenge (Figure 3G). Consistently, oxygen consumption was reduced in HSF1 FKO mice without alternations in NE levels in iWAT and serum, food intake, or locomotor activity, indicative of decreased energy expenditure in FKO mice (Figures 3H, S4I, and S4J). These differences were not caused by an enhancement in adipogenesis in

Statistical significance was assessed by two-way ANOVA followed with Bonferroni's multiple comparisons test (B–D, F, and G), ANCOVA with body weight as covariant (E) or unpaired Student's t test (H–J).
Data are presented as mean ± SEM and *$p < 0.05$ and **$p < 0.01$. Scale bars, 50 μm.
See also Figures S2 and S3 and Table S1.

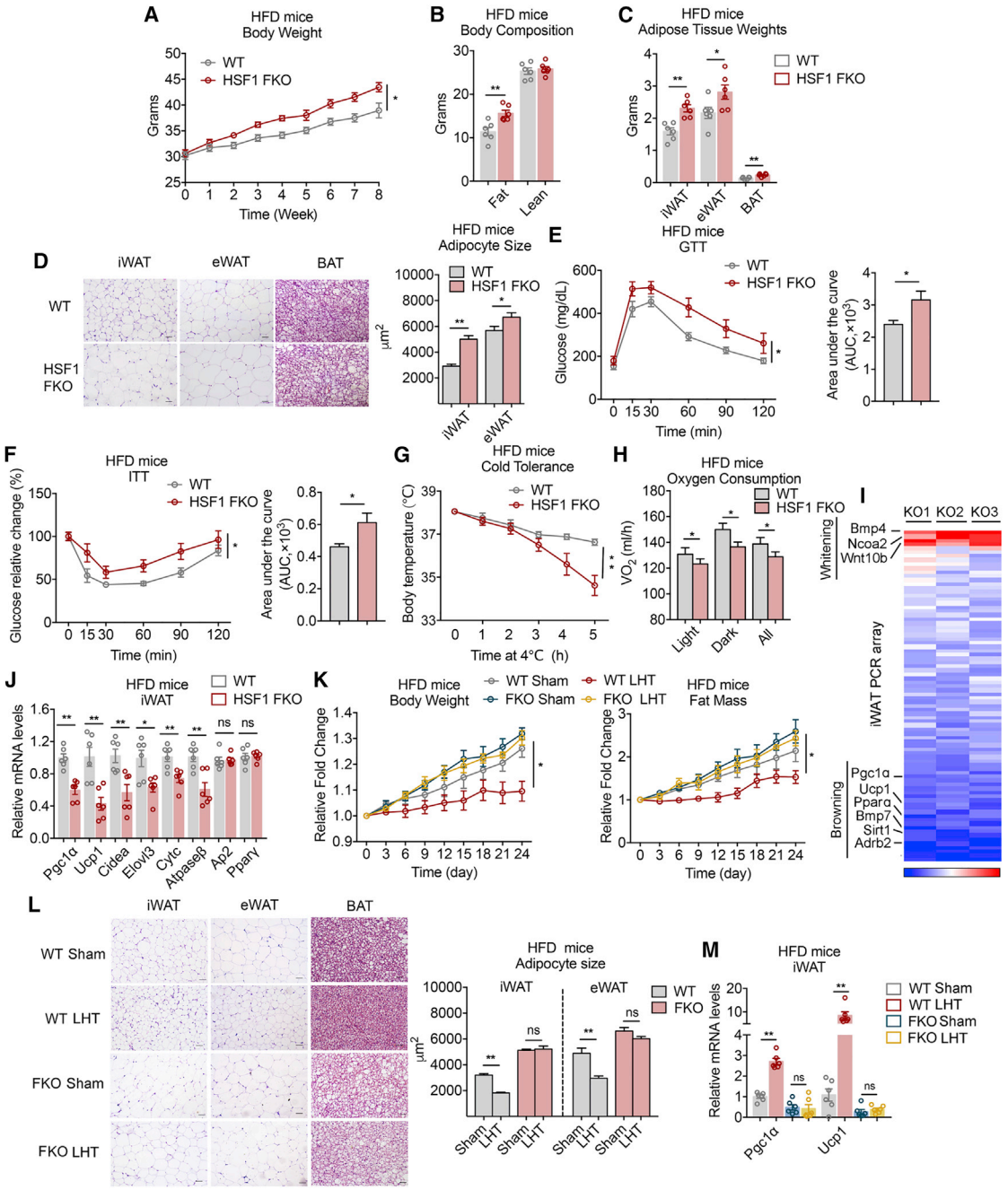

Figure 3. HSF1 regulates browning of white fat and is indispensable for the effects of LHT in adipocytes and in mice

(A–J) Analysis of metabolic parameters of wild-type (WT) and Adiponectin-Cre $Hsf1^{loxp/loxp}$ mice (HSF1 FKO) on 8 weeks of HFD; set the $Hsf1^{loxp/loxp}$ mice without Adiponectin-Cre as WT (n = 6), including (A) body weight; (B) body composition; (C) adipose tissue weights; (D) representative H&E staining of adipose tissues and adipocyte sizes; (E) GTT; (F) ITT; (G) cold tolerance test; (H) whole-body oxygen consumption; (I) PCR array analyzing adipocyte functionality in FKO iWAT normalized to individual gene levels in WT iWAT; (J) mRNA levels of thermogenic, mitochondrial, and adipogenic genes in iWAT.

(K–M) Analysis of metabolic parameters of WT and HSF1 FKO mice treated with Sham or LHT once every 3 days on HFD (n = 6), including (K) body weight and fat mass, (L) representative H&E staining of adipose tissues and quantification of average adipocyte sizes, and (M) mRNA levels of *Pgc1α* and *Ucp1* genes in iWAT. Statistical significance was assessed by two-way ANOVA followed with Bonferroni's multiple comparisons test (A, E–G, and K), ANCOVA with body weight as covariant (H) or unpaired Student's t test (B–D, J, L, and M). Data are presented as mean ± SEM and *p < 0.05 and **p < 0.01. Scale bars, 50 μm.

See also Figures S4 and S5.

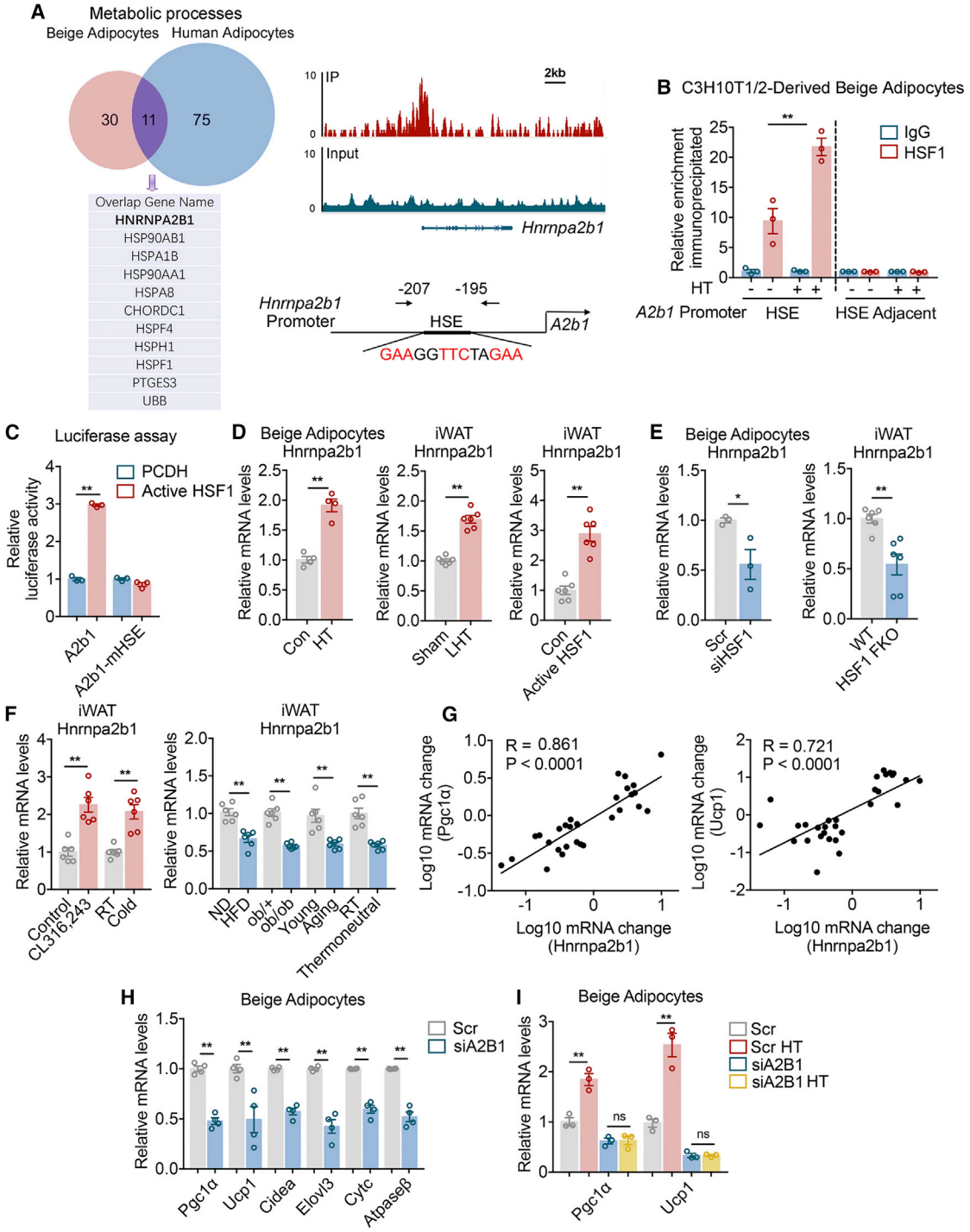

Figure 4. HSF1 controls *Hnrnpa2b1* transcription, and *Hnrnpa2b1* levels in beige adipocytes are associated with metabolic status

(A) Venn diagram of overlapped top metabolic processes genes from HSF1 ChIP-seq C3H10T1/2-derived beige adipocytes dataset (GSE176375) and human white adipocyte dataset (GSE24326) and a highly enriched binding of HSF1 on the promoter of *A2b1* at the putative HSE site.

(B) ChIP assay assessing HSF1 binding on the putative HSE region of the *A2b1* promoter in C3H10T1/2-derived beige adipocytes (n = 3).

(C) HSF1 activation induced wild-type *A2b1* transcriptional activity but not a HSE mutant reporter (*A2b1*-mHSE) (n = 3).

(D and E) mRNA level of *A2b1* following HSF1 activation or deficiency. (D) Control (Con) or HT-treated C3H10T1/2-derived beige adipocytes (left, n = 4); Sham- or LHT-treated iWAT of mice (middle, n = 6); AAV-mediated GFP (Con) or active form HSF1 (active HSF1) overexpression in iWAT of mice (right, n = 6); (E) scramble (Scr) or siHSF1 delivery into immortalized beige adipocytes (left, n = 3); iWAT from WT or HSF1 FKO mice (right, n = 6).

(legend continued on next page)

HSF1 FKO mice, since primary preadipocytes from WT and HSF1 FKO mice showed similar differentiation capacity *in vitro* (Figure S4K) and comparable expression levels of adipogenic gene programs were observed in adipose tissues of WT and HSF1 FKO mice (Figures 3J and S4L). Notably, PCR array analysis and subsequent qPCR assay showed that, compared with WT, HSF1 FKO mice exhibited significantly suppressed thermogenic and mitochondrial genes accompanied with elevated white gene programs in iWAT, but not in BAT (Figures 3I, 3J, and S4L).

Next, we investigated whether HSF1 plays an important role in mediating the metabolic benefits of LHT. As expected, LHT promoted significant metabolic improvements, including reduced body weighs, fat mass, and adipocyte sizes. However, these metabolic benefits of LHT were abrogated in HSF1 FKO mice, as FKO LHT and FKO Sham mice exhibited comparable increases in adiposity (Figures 3K and 3L). Further molecular analysis revealed that LHT failed to increase the expression levels of *Pgc1α* and *Ucp1* in FKO LHT mice as it did in WT LHT mice (Figure 3M). This was recapitulated in WT and HSF1 FKO mice under thermoneutral environment without impacts on angiogenic or inflammatory gene programs (Figures S4M and S4N). These results unveiled a critical role of HSF1 in mediating the metabolic benefits of LHT.

To further evaluate the role of HSF1 in LHT, we utilized an adenovirus-associated virus (AAV) overexpressing an active form of HSF1 (AAV Active HSF1), which lacks the LZ2 region critical for oligomerization repression and thus remains constantly active (Uchiyama et al., 2007), and delivered it in iWAT of mice to induce specific increase in HSF1 mRNA levels in beige fat (Figure S5A). AAV Active HSF1 delivery in iWAT largely recapitulated the metabolic improvements induced by LHT in HFD mice, as demonstrated by decreased body weights and fat mass, reduced adipose tissue weights and smaller adipocytes, improved serum lipid profiles, mitigated hepatic steatosis (Figures S5B–S5G), as well as improved insulin sensitivity (Figures S5H and S5I). Consistently, HSF1 activation in mice iWAT also increased their energy expenditure and cold tolerance capacity, as well as brown gene programs and PGC1α and UCP1 protein levels in iWAT of AAV Active HSF1 group compared with AAV GFP group (Figures S5J–S5M). These data suggest that fat-specific Active HSF1 overexpression mimics the metabolic actions of LHT through promoting white fat browning.

HSF1 controls *Hnrnpa2b1* transcription and Hnrnpa2b1 levels are associated with metabolic status in beige adipocytes

To further elucidate the mechanism of HSF1 in regulating beige fat activation, we performed ChIP-seq to access the genomic landscape of HSF1-binding targets in C3H10T1/2-derived beige adipocytes. Gene ontology analysis of HSF1 binding targets enriched functions closely related to metabolic processes (Table S2). To find direct target genes feature conserved metabolic regulation by HSF1, we cross-analyzed our in-house ChIP-seq dataset (GSE176375) from mice beige adipocytes with dataset from human adipocytes differentiated from mesenchymal stem cells (GSE24326) and focused on top genes involved in metabolic processes (Lo et al., 2011) (Figure 4A). A detailed analysis of overlapping genes showed that, in consistent with conventional HSF1 functionality, most of these HSF1 targets are involved in modulation of protein homeostasis, including classic HSF1 targets chaperon HSP90AB1, HSPA1B, HSP90AA1, HSPA8, HSP-interacting protein CHORDC1, HSPF4, HSPH1, HSPF1, co-chaperon PTGES3, as well as ubiquitin B (UBB), a peptide critical for protein ubiquitination and degradation. Intriguingly, the analysis also revealed a unique candidate, HNRNPA2B1 (A2B1), as the only RNA-binding protein and a potential HSF1 target, which piqued our interest (Figure 4A).

ChIP-seq analysis revealed specific enrichment of HSF1 binding on the *A2b1* promoter region, while *in silico* prediction revealed a classic heat-shock-factor-binding element (HSE) within this region (Figure 4A). Subsequent ChIP assay confirmed specific HSF1 binding on the predicted HSE region of *A2b1* promoter, but not on the adjacent region, in both C3H10T1/2-derived beige adipocytes and immortalized beige adipocytes. Importantly, this HSF1 binding is largely enhanced upon HT (Figures 4B and S5N). As shown in luciferase assay, overexpression of active form HSF1 significantly induced *A2b1* transcriptional activation, while this activation was lost by mutating the HSE site (mHSE) on the *A2b1* promoter (Figure 4C). Echoing the results of luciferase analysis, *in vitro* manipulation using hyperthermia on beige adipocytes, *in vivo* manipulations via LHT or AAV Active HSF1 in mice iWAT, all resulted in enhanced *A2b1* expression (Figure 4D), while HSF1 deficiency abrogated *A2b1* expression both *in vitro* and *in vivo*, as demonstrated using siHSF1 delivery into beige adipocytes or iWAT of HSF1 FKO mice (Figure 4E). Collectively, these results signified a possible HSF1-A2B1 axis upon LHT.

Next, we examined the involvement of A2B1 in beige fat function. Of note, we found that *A2b1* levels are tightly associated with beige fat function, as *A2b1* showed increased expressions in iWAT in conditions that promoting white fat browning, including CL316,243 treatment and cold stimulation (Figure 4F), while conversely, *A2b1* was downregulated in iWAT in scenarios that suppressing beige fat function, i.e., diet- (HFD) or genetic- (ob/ob) induced obese mice, aging mice, as well as mice under thermoneutral environment (Figure 4F). Furthermore, we found that there is a close correlation between *A2b1* mRNA levels

(F) mRNA level of *A2b1* in iWAT of β-adrenergic receptor agonist CL316,243 (CL) or cold-treated mice versus their controls (left, n = 6); iWAT of diet- (HFD) or genetic- (ob/ob) induced obese mice, aging mice, under thermoneutral condition versus their controls (right, n = 6). RT, room temperature.
(G) The correlation between *A2b1* and *Pgc1α* (left) or *Ucp1* (right) mRNA levels in mice iWAT (n = 30).
(H) mRNA levels of thermogenic and mitochondrial genes in immortalized beige adipocytes treated with scramble (Scr) and siA2B1 (n = 4).
(I) mRNA levels of *Pgc1α* and *Ucp1* in immortalized beige adipocytes treated with scramble (Scr) or siA2B1 under control or HT (n = 3).
Statistical significance was assessed by unpaired Student's t test (B–F, H, and I). Values were presented as Pearson's r correlation coefficient (G). Data are presented as mean ± SEM and *p < 0.05 and **p < 0.01.
See also Table S2.

with *Pgc1α* and *Ucp1* mRNA levels, respectively, in mice iWAT (Figure 4G). Functionally, A2B1 knockdown (siA2B1) decreased brown fat gene programs in beige adipocytes (Figure 4H). More importantly, HT-induced enhancement in *Pgc1α* and *Ucp1* expressions are at least partially dependent on A2B1 (Figure 4I). Overall, these results uncovered a previously unappreciated role of A2B1 in beige fat functions, as well as an indispensable role of the HSF1-A2B1 transcription axis in mediating beige fat activation by LHT.

HNRNPA2B1 promotes browning of white fat and energy metabolism

Next, we focused on assessing the physiological relevance of A2B1 in beige fat function and energy metabolism *in vivo*. We established a fat-specific A2B1 gain-of-function model by administrating an AAV carrying A2B1 construct (AAV A2B1) or control (AAV GFP) in mice iWAT. AAV A2B1 delivery achieved specific *A2b1* overexpression in iWAT (Figure S6A). When subjected to HFD, mice with fat-A2B1 overexpression showed significant decrease in body weights, fat mass, and adipose tissue weights with smaller adipocyte sizes (Figures 5A and 5B). They also featured increased oxygen consumption, enhanced resistance to cold challenge, as well as improved insulin sensitivity and hepatic steatosis (Figures 5C–5E and S6B). Both groups had similar food intake and locomotor activity (Figure S6C). Notably, AAV A2B1 group exhibited enhanced levels of brown gene programs, as well as increased PGC1α and UCP1 protein level in iWAT compared with AAV GFP group (Figure 5F).

On the other hand, we also studied the impact of HNRNPA2B1 loss of function on beige fat using mice injected with an AAV carrying shRNA targeting HNRNPA2B1 (AAV shA2B1) or control (AAV shNC) in iWAT. AAV shA2B1 delivery achieved specific knockdown of *A2b1* expression in iWAT (Figure S6D). Upon HFD, we observed opposite phenotypes in mice with fat-A2B1 knockdown compared with mice with fat-A2B1 overexpression. AAV shA2B1 mice showed increased body weights and adiposity, decreased oxygen consumption, impaired cold tolerance, as well as more severe insulin resistance and hepatic steatosis compared with AAV shNC mice (Figures 5G–5K and S6E), whereas both groups had similar food intake and locomotor activity (Figure S6F). A2B1 ablation in iWAT suppressed brown gene programs, as well as PGC1α and UCP1 protein levels, in AAV shA2B1 mice compared with control (Figure 5L).

To have a better understanding of the *in vivo* role of A2B1 on metabolic performances from a genetic point of view, we generated A2B1 haploinsufficient mice (A2B1 HET) that characterized an approximately 50% reduction in the *A2b1* level in adipose tissues, which mimics the organismal decrease of *A2b1* levels in response to physiological cues that suppress browning (Figure S6G). Under normal chow diet, A2B1 HET mice showed comparable body weights, adipose tissue weights, oxygen consumption, food intake, and locomotor activity to WT littermates (Figures S6H, S6I, and S6M). Intriguingly, we noticed that A2B1 HET mice featured increased adipocyte sizes in iWAT and impaired insulin sensitivity (Figures S6J–S6L), in accordance with suppressed brown gene programs in iWAT in these mice (Figure S6N). They also exhibited impaired thermogenic capacity as evident by more profound drops in core temperatures and blunted ability to induce *Pgc1α* and *Ucp1* expression in iWAT upon cold challenge (Figure S6O). These changes in A2B1 HET mice seems to be specific to beige fat, as their BAT showed no obvious mitigation on thermogenic gene programs or cold responses, indicating a unique role of A2B1 on beige fat functionality (Figures S6O and S6P).

Taken together, these results emphasized an indispensable and protective role of A2B1 against DIO and metabolic dysfunctions by promoting beige fat activation in mice.

HNRNPA2B1 acts downstream of HSF1 to enhance the stability of metabolic gene transcripts

We then set out to unravel the role of A2B1 in mediating the metabolic functions of HSF1 in adipocytes. To achieve this, we overexpressed A2B1 via AAV A2B1 or vector via AAV GFP in iWAT of HSF1 FKO mice (FKO + A2B1, FKO + GFP) and compared them with WT mice treated with AAV GFP (WT + GFP). Upon HFD feeding, evaluation of metabolic parameters revealed that A2B1 overexpression in fat largely alleviated the metabolic impairments of HSF1 FKO mice (Figures 6A–6G). Furthermore, ectopic expression of A2B1 in iWAT of HSF1 FKO mice rescued the decreased expression of thermogenic genes in HSF1 FKO mice (Figure 6H). These data suggest that HSF1-A2B1 axis regulates browning of white fat to protect against obesity and metabolic dysfunction.

A2B1 is an RNA-binding protein that has been reported to be critical for miRNA maturation and mRNA splicing and processing (Alarcón et al., 2015; Geissler et al., 2016; Martinez et al., 2016; Wang et al., 2019). To decipher the exact regulatory mechanism of A2B1 in beige fat function, we first examined the levels of miR324, miR93, miR222, and miR106b, the miRNAs reported to be modulated by A2B1, upon A2B1 overexpression or knockdown (Alarcón et al., 2015). We found that perturbation of A2B1 levels failed to impact these miRNA levels, indicating that A2B1 may not affect miRNAs in beige fat (Figure S7A). We then performed RNA-seq analysis using iWAT from fat-specific A2B1 overexpression mice or control mice. A detailed analysis of enriched gene sets impacted by A2B1 revealed that A2B1 caused more profound alterations in transcriptional events than splicing events (around 4-fold) (Figure S7B). Furthermore, Kyoto Encyclopedia of Genes and Genomes (KEGG) analysis on oscillating genes that underwent transcriptional changes enriched for metabolism as top one pathway (Figure S7C, left), while KEGG analysis on gene sets that underwent splicing events enriched pathways unrelated to lipid and glucose metabolism (Figure S7C, right). Overall, these results indicate that the regulation of A2B1 on beige fat function may through its impact on lipid and glucose metabolic gene expression rather than splicing or miRNA processing.

A2B1 has been reported to function as a m6A reader by binding to the 3′ untranslated region (3′ UTR) of target mRNAs and subsequently impact mRNA destiny, i.e., mRNA stability and mRNA translocation (Wang et al., 2019). Sequence analysis showed the existence of specific A2B1-binding site on 3′ UTR of key genes in browning programs, including *Pgc1α*, *Ucp1*, *Elovl3*, and *Cytc*, which was confirmed by RNA immunoprecipitation (RIP) analysis (Figure 6I). We further demonstrated that in beige adipocytes, A2B1 overexpression significantly increased

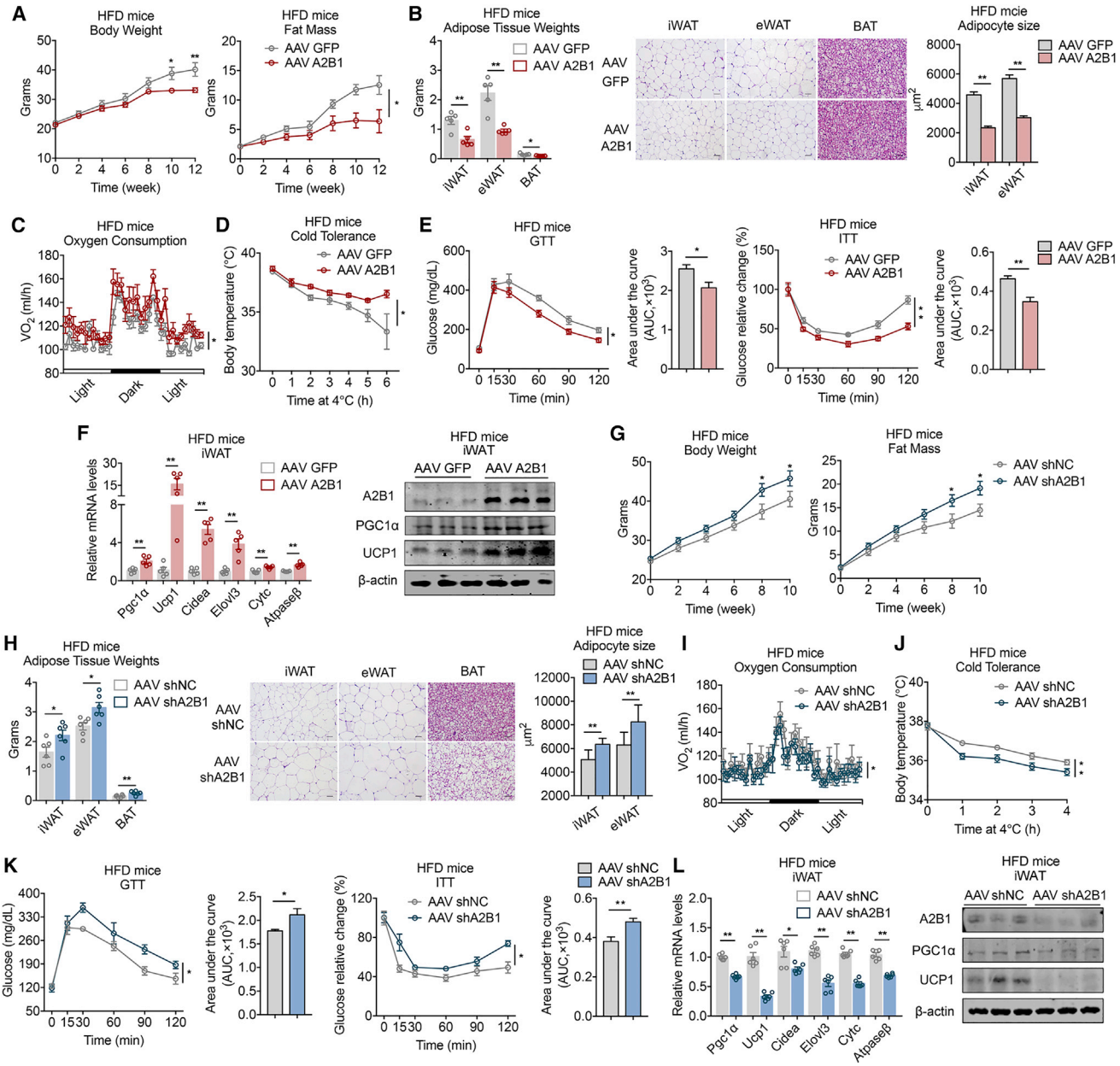

Figure 5. HNRNPA2B1 promotes browning of white fat and energy metabolism

(A–L) Analysis of metabolic parameters of C57BL/6J mice on HFD with iWAT injection of AAV-mediated GFP (AAV GFP) or A2B1 overexpression (AAV A2B1) (A–F, n = 5), or AAV-mediated scrambled control (AAV shNC) or HNRNPA2B1 knockdown (AAV shA2B1) (G–L, n = 6), including (A and G) body weight and fat mass; (B and H) adipose tissue weights, representative H&E staining of adipose tissues; (C and I) whole-body oxygen consumption; (D and J) cold tolerance test; (E and K) GTT and ITT; (F and L) mRNA levels of thermogenic and mitochondrial genes in iWAT; immunoblotting for A2B1, PGC1α, and UCP1 protein levels in iWAT. Statistical significance was assessed by unpaired Student's t test (A, B, F–H, and L), ANCOVA with body weight as covariant (C and I) or two-way ANOVA followed with Bonferroni's multiple comparisons test (A, D, E, J, and K). Scale bars, 50 μm. Data are presented as mean ± SEM and *p < 0.05 and **p < 0.01.
See also Figure S6.

the luciferase activity of a luc-reporter construct containing *Pgc1α* 3′ UTR (3′ UTR-WT), while deletion of the A2B1 binding site in *Pgc1α* 3′ UTR (3′ UTR-DEL) abrogated this activation, whereas assays using *Ucp1* 3′ UTR-WT and *Ucp1* 3′ UTR-DEL rendered similar effects (Figure 6J). Importantly, A2B1 knockdown reduced, while A2B1 overexpression extended, the mRNA stability of *Pgc1α*, *Ucp1*, *Elovl3*, and *Cytc*, suggesting that A2B1 may function through recognizing and binding to mRNAs of a specific set of key browning genes to enhance their mRNA stability (Figures 6K, 6L, S7D, and S7E). In addition, consistent with the role of A2B1 as a downstream mediator of HSF1 in regulating beige fat function, we found that HSF1

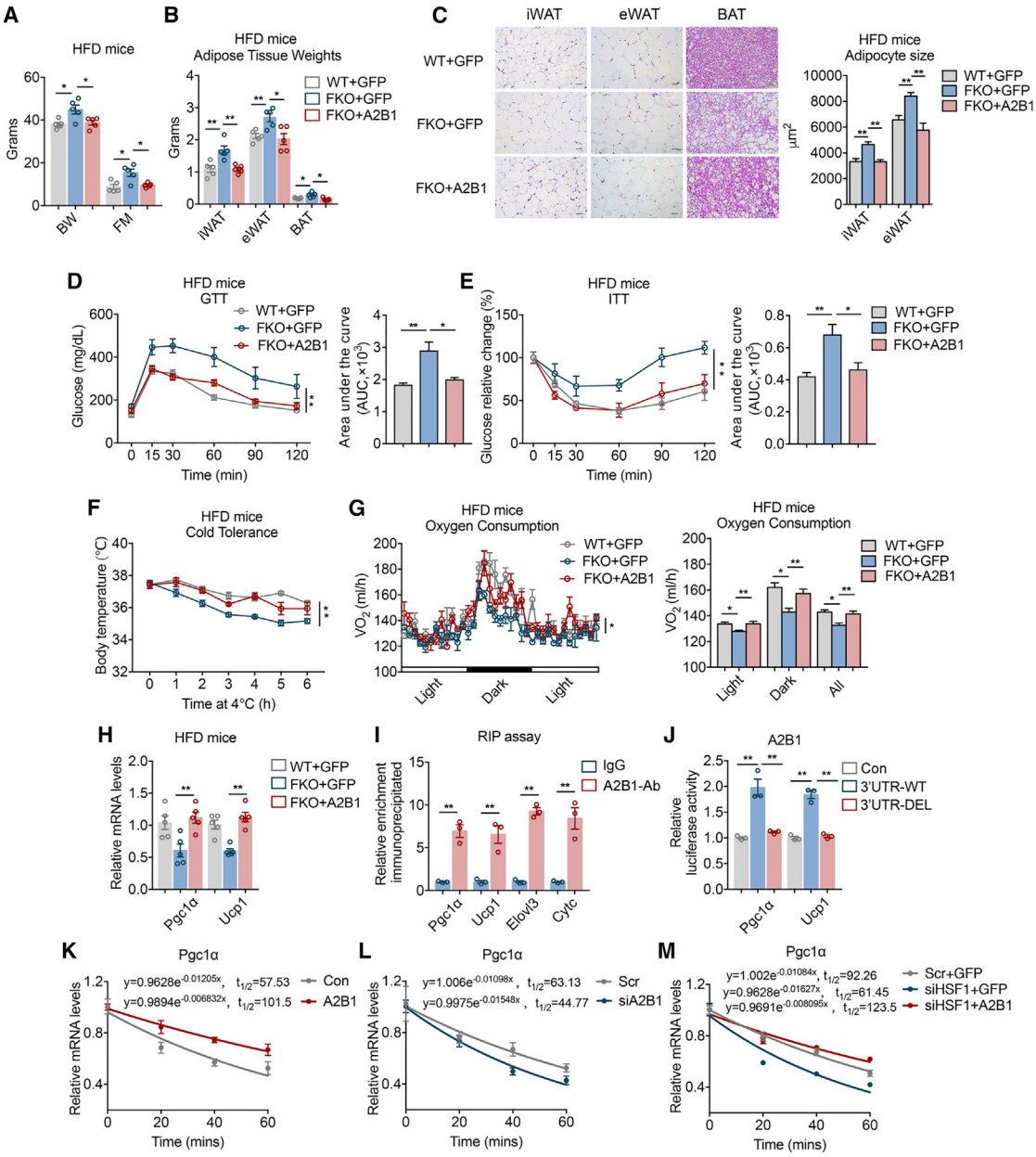

Figure 6. HNRNPA2B1 acts downstream of HSF1 to enhance the stability of metabolic gene transcripts

(A–H) Analysis of metabolic parameters of AAV-mediated GFP overexpression in iWAT of WT mice on HFD, or GFP, or A2B1 overexpression in iWAT of HSF1 FKO mice on HFD (n = 5), including (A) body weight (BW) and fat mass (FM); (B) adipose tissue weights; (C) representative H&E staining of adipose tissues; (D) GTT; (E) ITT; (F) cold tolerance test; (G) oxygen consumption; (H) mRNA levels of *Pgc1α* and *Ucp*1 in iWAT.

(I) RNA immunoprecipitation (RIP) assay assessing A2B1 binding on 3′UTR of *Pgc1α*, *Ucp1*, *Elovl3*, and *Cytc* in immortalized beige adipocytes (n = 3).

(J) A2B1 overexpression induces *Pgc1α* and *Ucp1* wild-type 3′UTR transcriptional activity (*Pgc1α*/*Ucp1* 3′UTR-WT) but not promoters with the deletion of the putative A2B1-binding site on *Pgc1α* or *Ucp1* 3′UTR (*Pgc1α*/*Ucp1* 3′UTR-DEL) (n = 3).

(K–M) mRNA level of Pgc1α in (K) control (Con) or A2B1 overexpression, (L) scramble (Scr) or A2B1 knockdown (siA2B1) and (M) ADV mediated GFP or A2B1 overexpression co-treated with scramble (Scr) and siHSF1 immortalized beige adipocytes upon transcriptional inhibition with actinomycin D at indicated time (n = 4).

Statistical significance was assessed by unpaired Student's t test (A–C and H–M), two-way ANOVA followed with Bonferroni's multiple comparison test (D–F) or ANCOVA with body weight as covariant (G). Data are presented as mean ± SEM and *p < 0.05 and **p < 0.01. Scale bars, 50 μm.

See also Figure S7.

deficiency reduced half-life of *Pgc1α*, *Ucp1*, *Elovl3*, and *Cytc* mRNA, which was reversed upon A2B1 overexpression (Figures 6M and S7F). Interestingly, we found that *Hsf1* and *A2b1* mRNA levels, as well as A2B1-binding activities on thermogenic genes were higher in beige fat versus brown fat, which may partially explain the differential responses of beige and brown fat to LHT (Figures S7G and S7H). Overall, these results support that A2B1 may regulate beige fat functions by binding to the 3′ UTR of key browning genes to enhance their mRNA stability.

The association of HSF1 variant P365T with human metabolic traits

For clinical relevance, we explored the association of HSF1 genetic variants (single-nucleotide polymorphisms, SNPs) with metabolic traits in humans. Interestingly, using previously reported genome-wide association study (GWAS) datasets from Shanghai Nicheng Cohort Study (Chen et al., 2018) and exome-wide association study datasets from Shanghai Fat Distribution and Disease (FADE) (Bao et al., 2013), we identified a missense variant p.Pro365Thr (c.1093C>A, rs78202224) in exon 9 of the *HSF1* gene (Figure 7A). The genotype distribution was 9,380 subjects (93.04%) with CC, 688 subjects (6.82%) with AC, and 14 subjects (0.14%) with AA. The characteristics of different genotype subjects are shown in Table S3. Of note, the carrying of A allele in subjects was associated with mild but significant decrease in body mass index (BMI) and serum total triglyceride (Figures 7B and 7C). Besides, subjects with A allele also had significantly lowered fasting glucose, lower plasma glucose levels after oral glucose tolerance test (OGTT), and lower γ-glutamyltranspeptidase (Figures 7D–7G). Multiple linear regression adjusting for age and sex showed that rs78202224-A was negatively associated with BMI ($\beta = -0.25$, se = 0.12, p = 0.0478), serum total triglyceride ($\beta = -0.02$, se = 0.01, p = 0.0304), fasting plasma glucose ($\beta = -0.07$, se = 0.02, p = 0.0014), 2-h plasma glucose ($\beta = -0.38$, se = 0.07, $p = 2.12 \times 10^{-8}$), glucose area under the curve (AUC) after OGTT ($\beta = -27.88$, se = 6.22, $p = 7.51 \times 10^{-6}$), and γ-glutamyltranspeptidase ($\beta = -3.67$, se = 1.18, p = 0.0019). Importantly, subsequent molecular studies revealed that the missense variant p.Pro365Thr (HSF1 AA) exhibited stronger activation effects on *A2b1* transcription than its WT counterpart (HSF1 CC) in the luciferase assay, while HSE mutation abrogated the effect (Figure 7H). Besides, HSF1 AA also promoted *A2b1* levels and brown fat gene programs more extensively than HSF1 CC in beige adipocytes or in mice iWAT, without affecting adipogenic genes (Figures 7I and 7J). Overall, these results demonstrate the potential contribution of HSF1 in human metabolism and that HSF1 activation may serve as a promising target in preventing and treating obesity.

DISCUSSION

In this study, we achieved localized LHT on beige adipocytes *in vivo* using PEG-PDA hydrogel. PDA is a very safe and biocompatible photothermal agent that can efficiently convert NIR light input into local heat output (Cheng et al., 2019; Liu et al., 2014; Zhou et al., 2017). Moreover, PEG-PDA hydrogel is used here to facilitate the repeated light illuminations in a long period (Wang et al., 2016b). Consistently, we found no adverse effects of mice injected with PDA upon long-term observation. Of note, this study offered a proof of concept of LHT of beige fat in treating obesity and metabolic diseases. It would be worthwhile to utilize newly developed ways of PDA delivery methods, including nanopatch for needle-free and painless delivery, or other new nanomaterials capable of precise temperature control to achieve improved ways of LHT in beige fat, including in human.

The impacts of thermal stress have recently been studied on various immune cells (Lin et al., 2019; O'Sullivan et al., 2021; Wang et al., 2020). Although the thermal stress used in these studies (39°C–40°C) seemed lower than that in our study (41°C ± 0.5°C), it should be noted that these studies are conducted in the context of fever; thus, the thermal stress reflects a significant change in core temperature, whereas in our study, the thermal stress is locally applied, without affecting core temperature in human or mice. Importantly, the increasing of LHT-induced local temperature to 41°C ± 0.5°C in this study did not cause overt stress to skin or adjacent tissues, as similar or even higher temperature was generally used in studies of whole-body HT in mice and in humans (Chung et al., 2008; Fu et al., 2010; Boreham et al., 1995; Kihara et al., 2002; Thomas et al., 2017), which supported the safeness of the temperature and treating duration in our study. In addition, we have shown that LHT did not alter NE levels, NE turnover rate, or cortisol levels in mice and human subjects, overall suggesting the safeness of 41°C ± 0.5°C LHT *in vivo*. Interestingly, it has been shown that severe burn induces browning of white fat in mice and humans via adrenergic stress and inflammation (Abdullahi et al., 2019; Patsouris et al., 2015; Vinaik et al., 2019). Although we have eliminated a potential contribution of macrophages and stress hormones in the browning effect of LHT, it would be necessary to study the roles of other immune cells in the process of LHT, as well as the possible involvement of HSF1-A2B1 axis in burning-induced fat browning. Besides, future work on other possible mechanisms of LHT on metabolic improvements, including enhanced lipids secretion through skin (Choa et al., 2021) or adipose-tissue-intestine crosstalk (Zhang et al., 2021), microbiota composition and metabolomics, may provide more information.

Interestingly, we observed different responses of beige and brown fat to LHT, which may at least partially due to the higher expression levels of *Hsf1* and *A2b1*, as well as the greater A2B1-binding activities on thermogenic genes in beige adipocytes than brown adipocytes, Besides, previous studies using transponder probe implantation in brown fat indicated that BAT temperature is higher than core body temperature and would experience further elevation upon activation (Ikeda et al., 2017; Lute et al., 2014). Thus, BAT may be relatively insensitive to LHT compared with iWAT. In addition, high-throughput analysis and studies with genetic animal models suggested that although the majority of the gene programs or proteins are similar, there are no doubt that distinct signatures between iWAT and BAT exist (Kazak et al., 2015; Long et al., 2014; Cohen et al., 2014; Kleiner et al., 2012), which may underlie their different responses to stimuli.

Recently, we and other groups have revealed the existence of HSF1-PGC1α transcriptional axis in multiple organs including fat, muscle, liver, and brain (Gomez-Pastor et al., 2017; Ma

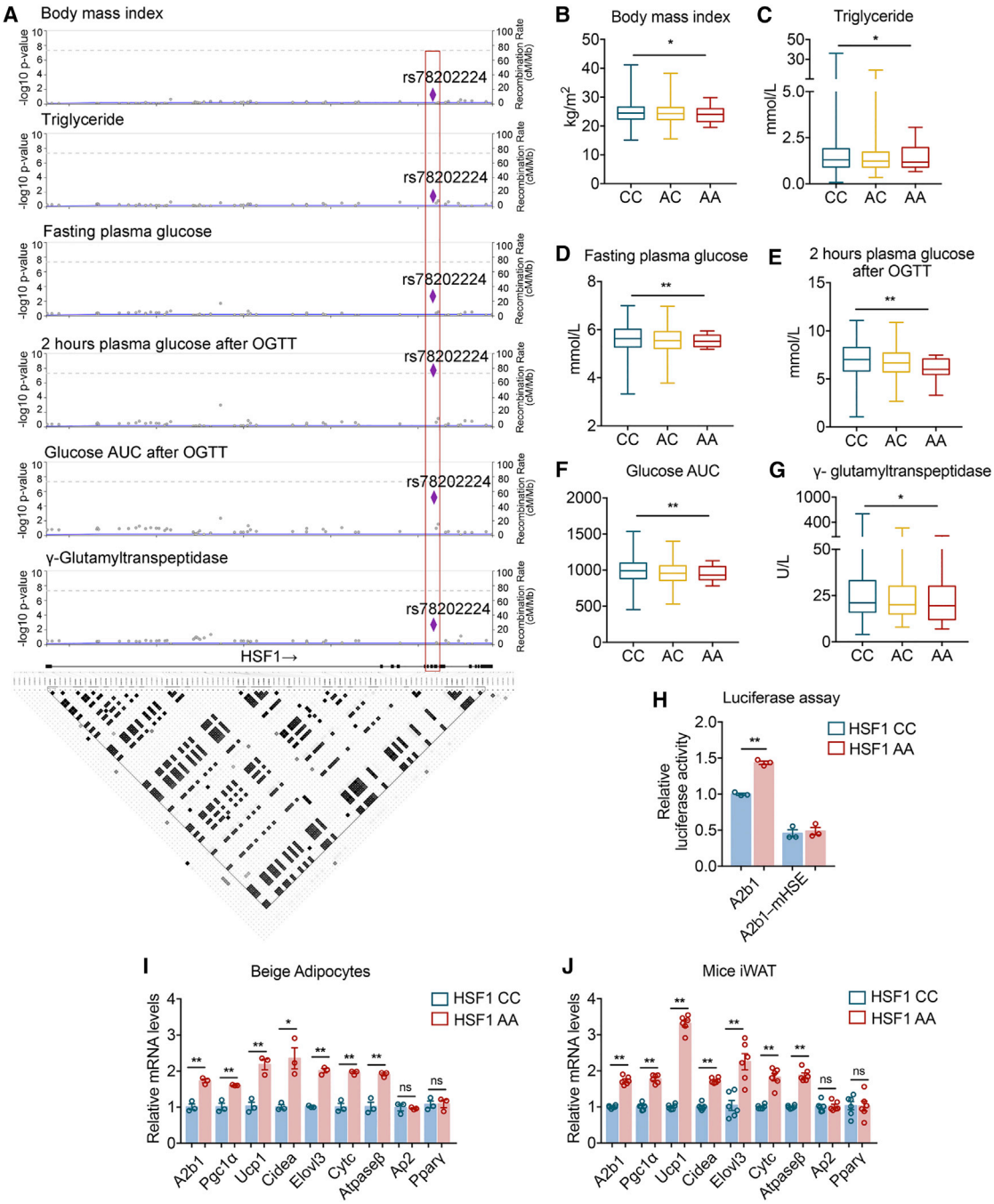

Figure 7. The association of HSF1 with human metabolic traits

(A) Region plot shows the association between genetic variants in the *HSF1* gene region (SNP, p.Pro365Thr, rs78202224) with body mass index (BMI), triglyceride, fasting plasma glucose, 2-h plasma glucose after oral glucose tolerance test (OGTT), area under curve (AUC) of glucose after OGTT and γ-glutamyltranspeptidase. Genome build is aligned with the GRCh37/hg19 assembly. Linkage disequilibrium of variants is calculated based on East-Asian population from 1000 Genomes project phase III.

(B–G) Association between rs78202224 (CC, wild-type; AC, heterozygous; AA, mutation) with (B) body mass index; (C) serum total triglyceride levels; (D) fasting plasma glucose levels; (E) 2-h plasma glucose levels after OGTT; (F) AUC of glucose after OGTT; (G) γ-glutamyltranspeptidase levels.

(H) HSF1 wild-type (CC) and Pro365Thr variant (AA) overexpression for *Hnrnpa2b1* luciferase transcriptional activities (n = 3).

(I and J) mRNA levels of brown fat gene programs and adipogenic genes in immortalized beige adipocytes (n = 3) or mice of iWAT (n = 6) expressing HSF1 wild-type (CC) or Pro365Thr variant (AA).

Linear regression analysis was used to test for the effects of SNP on quantitative traits under the additive genetic model (B–G). Statistical significance was assessed by unpaired Student's t test (H–J). Data are presented as mean ± SEM and *p < 0.05 and **p < 0.01.

See also Table S3.

et al., 2015; Qiao et al., 2017). In this study, we performed ChIP-seq to evaluate the regulatory network of HSF1 on genomic scale and revealed a HSF1-A2B1 axis that impacts the mRNA stability of various key metabolic genes, including PGC1α. Thus, HSF1 may regulate *Pgc1α* levels at both transcriptional and post-transcriptional level for stress responses, which may be vital in maintaining cellular homeostasis, as well as in pathological states where HSF1-A2B1 axis is damaged, i.e., through obesity and aging. Moreover, besides *Pgc1α*, we further identified *Ucp1* as a target of HSF1-A2B1 axis, suggesting a previously unappreciated broader role of HSF1 in metabolic control. Future work on a comprehensive picture of HSF1's function in energy metabolism is warranted.

An interesting observation of this study is that hyperthermia induces thermogenesis by activating beige fat. This seemingly contradictory phenomenon could be explained by a role of HSF1 in mitohormesis (Labbadia et al., 2017; Tharp et al., 2021). In this sense, heat stress has been shown to induce mitochondrial reactive oxygen species (ROS) production (Yu et al., 2019). Unchecked ROS production causes cell death in the scenario of lethal high temperature, while non-lethal hyperthermia causes perturbation, which activates HSF1 and triggers mitohormesis with long-term beneficial effects for cellular and organismal health (Labbadia et al., 2017; Tharp et al., 2021; Yun and Finkel, 2014). Of note, PGC1α, a strong inducer of mitochondrial biogenesis, has been shown to induce a potent antioxidant stress resistance program, i.e., in brain and heart, thus promote mitochondrial ROS balance (Bouitbir et al., 2012; St-Pierre et al., 2006). Meanwhile, UCP1 is reported to enhance mitochondrial proton leak and inhibit mitochondrial ROS production through a feedback mechanism (Chan et al., 2010; Hoerter et al., 2004). Thus, it is possible that hyperthermia induces the mitohormesis response through HSF1 activation to restore mitochondrial ROS balance through its regulation of *Pgc1α* and *Ucp1*, which in turn enhances thermogenesis as their innate functions. Consistent with this notion, it has been demonstrated that mitochondrial ROS induces UCP1 Cys253 sulfenylation and UCP1 activation (Chouchani et al., 2016), which also point to a potential link between hyperthermia and thermogenesis via mitochondria ROS levels. Meanwhile, HSF1 activation may promote metabolic benefits through its role as a mitohormesis inducer via multiple mechanism, i.e., protection of protein homeostasis and restoring cellular redox balance.

Of clinical significance, we revealed the association of a gain-of-function HSF1 missense variant p. Pro365Thr with improved human BMI and metabolic traits. Interestingly, the variant characterized Pro365Thr substitution in the regulatory domain (RD) of HSF1. The activity of HSF1 has been reported to be regulated by various post-translational modifications including acetylation, phosphorylation, and sumoylation in its RD (Gomez-Pastor et al., 2018). Of note, HSF1 hyperphosphorylation has been shown to result in HSF1 transactivation under heat shock or its agonist celastrol treatment (Holmberg et al., 2001; Soncin et al., 2003; Westerheide et al., 2004), while phosphorylation of various sites within HSF1 RD, i.e., S363 and T367, have been reported to negatively regulate HSF1 transcriptional activity (Asano et al., 2016; Chu et al., 1998). The HSF1 Pro365Thr variant falls within S363 and T367, two negative regulatory phosphorylation sites. Threonine is an amino acid residue frequently subjected to phosphorylation modification. It is thus possible that Pro365Thr mutation results in a positive regulatory phosphorylation site in RD, thus enhancing HSF1 transcriptional activity, or interfering S363/T367 phosphorylation and blunting their repressive function. Although the structure of HSF1 N-terminal DNA-binding domain has been solved, the crystal structure of its RD domain remains a mystery (Neudegger et al., 2016). It would be interesting to perform future structural study to clarify the exact function of HSF1 Pro365Thr variant.

Limitations of the study

The major finding of this work signifies LHT as a promising strategy against obesity by inducing beige fat activation via the HSF1-A2B1 transcriptional axis. Future studies to investigate other possible mechanisms for the beneficial effects of LHT would provide more comprehensive understanding. Besides, it would be interesting to further understand the mechanisms underneath the differential responses of beige and brown fat under LHT. Additionally, it would be important to generate humanized knockin mice to provide genetic evidences of HSF1 SNPs on energy metabolism. Further clinical studies are warranted to investigate the long-term effects of LHT on weight control and metabolic parameters in obese or diabetic patients.

STAR★METHODS

Detailed methods are provided in the online version of this paper and include the following:

- KEY RESOURCES TABLE
- RESOURCE AVAILABILITY
  - Lead contact
  - Materials availability
  - Data and code availability
- EXPERIMENTAL MODEL AND SUBJECT DETAILS
  - Animals
  - Local hyperthermia therapy in mice
  - Local delivery of adeno-associated virus (AAV) in adipose tissues
  - Macrophage depletion in adipose tissues
  - Local hyperthermia therapy in human subjects
  - Human participants for genotyping
  - Differentiated adipocytes
- METHOD DETAILS
  - Metabolic analysis in mice
  - Thermal image analysis
  - Measurement of NE turnover
  - Blood flow measurements in mice
  - Fecal bomb calorimetry
  - Lentivirus-mediated gene transfer
  - Plasmid construction
  - RNA Extraction, quantitative PCR, PCR array, and RNA-seq
  - Immunoblotting
  - Immunofluorescence
  - Oil Red O staining and quantitative analysis
  - ChIP and ChIP-seq assays

- RNA immunoprecipitation assay
- Luciferase reporter assay
- Histological analysis
- Preparation of PDA-PEG hydrogel
- siRNA transfection
- RNA stability assay

- QUANTIFICATION AND STATISTICAL ANALYSIS

SUPPLEMENTAL INFORMATION

Supplemental information can be found online at https://doi.org/10.1016/j.cell.2022.02.004.

ACKNOWLEDGMENTS

We are grateful to Shanghai Fat Distribution and Disease (FADE) for assistance with human study and clinical data resources. We acknowledge Dr. Richard L. Prioa and Dr. Elisabetta Mueller from NIDDK, NIH for generously sharing HSF1 loxp mice and Dr. Yiyun Cheng (ECNU) for technique advice on photothermal therapy. This work was supported by funds from the National Natural Science Foundation of China (32022034, 31770840, 32071148, 31800989, and 81902980), the National Key Research and Development Program of China (2019YFA0904500 and 2018YFC1313800), the Shanghai Outstanding Academic Leaders (20XD1433300), the Shuguang Project (21SG11), the ECNU Public Platform for Innovation (011), and the Instruments Sharing Platform of School of Life Sciences.

AUTHOR CONTRIBUTIONS

Conceptualization, X.M. and L.X.; methodology, X.M., L.X., C.H., Q.Z., Y.L., and D.W; investigation, Y.L., D.W., X.P., Y.Z., T.Z., W.Z., M.G., F.S., M.M., X.C., and Y.Z.; resources, L.W., L.J., J.W., D.L., Q.Z., C.H., L.X., and X.M.; writing and editing, X.M., L.X., Y.L., D.W., X.P., Y.Z., C.H., Q.Z., and J.W.; project administration, X.M., L.X., C.H., and Q.Z.; funding acquisition, X.M., L.X., C.H., and D.W.; supervision, X.M., L.X., C.H., and Q.Z. All authors read and approved the manuscript.

DECLARATION OF INTERESTS

The authors declare no competing interests.

Received: September 20, 2021
Revised: December 28, 2021
Accepted: February 2, 2022
Published: March 4, 2022

REFERENCES

Abdullahi, A., Auger, C., Stanojcic, M., Patsouris, D., Parousis, A., Epelman, S., and Jeschke, M.G. (2019). Alternatively activated macrophages drive browning of white adipose tissue in burns. Ann. Surg. *269*, 554–563. https://doi.org/10.1097/SLA.0000000000002465.

Abreu-Vieira, G., Hagberg, C.E., Spalding, K.L., Cannon, B., and Nedergaard, J. (2015). Adrenergically stimulated blood flow in brown adipose tissue is not dependent on thermogenesis. Am. J. Physiol. Endocrinol. Metab. *308*, E822–E829. https://doi.org/10.1152/ajpendo.00494.2014.

Alarcón, C.R., Goodarzi, H., Lee, H., Liu, X., Tavazoie, S., and Tavazoie, S.F. (2015). HNRNPA2B1 is a mediator of m^{6}A-dependent nuclear RNA processing events. Cell *162*, 1299–1308. https://doi.org/10.1016/j.cell.2015.08.011.

Andrews, S. (2010). FastQC: a quality control tool for high throughput sequence data (Babraham Bioinformatics). http://www.bioinformatics.babraham.ac.uk/projects/fastqc/.

Archer, A.E., Rogers, R.S., Von Schulze, A.T., Wheatley, J.L., Morris, E.M., McCoin, C.S., Thyfault, J.P., and Geiger, P.C. (2018). Heat shock protein 72 regulates hepatic lipid accumulation. Am. J. Physiol. Regul. Integr. Comp. Physiol. *315*, R696–R707. https://doi.org/10.1152/ajpregu.00073.2018.

Asano, Y., Kawase, T., Okabe, A., Tsutsumi, S., Ichikawa, H., Tatebe, S., Kitabayashi, I., Tashiro, F., Namiki, H., Kondo, T., et al. (2016). IER5 generates a novel hypo-phosphorylated active form of HSF1 and contributes to tumorigenesis. Sci. Rep. *6*, 19174. https://doi.org/10.1038/srep19174.

Baird, N.A., Douglas, P.M., Simic, M.S., Grant, A.R., Moresco, J.J., Wolff, S.C., Yates, J.R., 3rd, Manning, G., and Dillin, A. (2014). HSF-1-mediated cytoskeletal integrity determines thermotolerance and life span. Science *346*, 360–363. https://doi.org/10.1126/science.1253168.

Bakker, L.E., Boon, M.R., van der Linden, R.A., Arias-Bouda, L.P., van Klinken, J.B., Smit, F., Verberne, H.J., Jukema, J.W., Tamsma, J.T., Havekes, L.M., et al. (2014). Brown adipose tissue volume in healthy lean South Asian adults compared with white Caucasians: a prospective, case-controlled observational study. Lancet Diabetes Endocrinol. *2*, 210–217. https://doi.org/10.1016/S2213-8587(13)70156-6.

Baler, R., Dahl, G., and Voellmy, R. (1993). Activation of human heat shock genes is accompanied by oligomerization, modification, and rapid translocation of heat shock transcription factor HSF1. Mol. Cell. Biol. *13*, 2486–2496. https://doi.org/10.1128/mcb.13.4.2486-2496.1993.

Bao, Y., Ma, X., Yang, R., Wang, F., Hao, Y., Dou, J., He, H., and Jia, W. (2013). Inverse relationship between serum osteocalcin levels and visceral fat area in Chinese men. J. Clin. Endocrinol. Metab. *98*, 345–351. https://doi.org/10.1210/jc.2012-2906.

Barbatelli, G., Murano, I., Madsen, L., Hao, Q., Jimenez, M., Kristiansen, K., Giacobino, J.P., De Matteis, R., and Cinti, S. (2010). The emergence of cold-induced brown adipocytes in mouse white fat depots is determined predominantly by white to brown adipocyte transdifferentiation. Am. J. Physiol. Endocrinol. Metab. *298*, E1244–E1253. https://doi.org/10.1152/ajpendo.00600.2009.

Baskaran, P., Krishnan, V., Ren, J., and Thyagarajan, B. (2016). Capsaicin induces browning of white adipose tissue and counters obesity by activating TRPV1 channel-dependent mechanisms. Br. J. Pharmacol. *173*, 2369–2389. https://doi.org/10.1111/bph.13514.

Bhadada, S.V., Patel, B.M., Mehta, A.A., and Goyal, R.K. (2011). β(3) receptors: role in cardiometabolic disorders. Ther. Adv. Endocrinol. Metab. *2*, 65–79. https://doi.org/10.1177/2042018810390259.

Boreham, D.R., Gasmann, H.C., and Mitchel, R.E. (1995). Water bath hyperthermia is a simple therapy for psoriasis and also stimulates skin tanning in response to sunlight. Int. J. Hyperthermia *11*, 745–754. https://doi.org/10.3109/02656739509052332.

Bouitbir, J., Charles, A.L., Echaniz-Laguna, A., Kindo, M., Daussin, F., Auwerx, J., Piquard, F., Geny, B., and Zoll, J. (2012). Opposite effects of statins on mitochondria of cardiac and skeletal muscles: a 'mitohormesis' mechanism involving reactive oxygen species and PGC-1. Eur. Heart J. *33*, 1397–1407. https://doi.org/10.1093/eurheartj/ehr224.

Brunt, V.E., Eymann, T.M., Francisco, M.A., Howard, M.J., and Minson, C.T. (2016). Passive heat therapy improves cutaneous microvascular function in sedentary humans via improved nitric oxide-dependent dilation. J. Appl. Physiol. (1985) *121*, 716–723. https://doi.org/10.1152/japplphysiol.00424.2016.

Butler, A.A., and Kozak, L.P. (2010). A recurring problem with the analysis of energy expenditure in genetic models expressing lean and obese phenotypes. Diabetes *59*, 323–329. https://doi.org/10.2337/db09-1471.

Caterina, M.J., Schumacher, M.A., Tominaga, M., Rosen, T.A., Levine, J.D., and Julius, D. (1997). The capsaicin receptor: a heat-activated ion channel in the pain pathway. Nature *389*, 816–824. https://doi.org/10.1038/39807.

Chan, S.L., Wei, Z., Chigurupati, S., and Tu, W. (2010). Compromised respiratory adaptation and thermoregulation in aging and age-related diseases. Ageing Res. Rev. *9*, 20–40. https://doi.org/10.1016/j.arr.2009.09.006.

Chen, L., Zhang, J., Zou, Y., Wang, F., Li, J., Sun, F., Luo, X., Zhang, M., Guo, Y., Yu, Q., et al. (2021). Kdm2a deficiency in macrophages enhances thermogenesis to protect mice against HFD-induced obesity by enhancing H3K36me2 at the pparg locus. Cell Death Differ. *28*, 1880–1899. https://doi.org/10.1038/s41418-020-00714-7.

Chen, P., Hou, X., Hu, G., Wei, L., Jiao, L., Wang, H., Chen, S., Wu, J., Bao, Y., and Jia, W. (2018). Abdominal subcutaneous adipose tissue: a favorable adipose depot for diabetes? Cardiovasc. Diabetol. *17*, 93. https://doi.org/10.1186/s12933-018-0734-8.

Cheng, W., Zeng, X., Chen, H., Li, Z., Zeng, W., Mei, L., and Zhao, Y. (2019). Versatile polydopamine platforms: synthesis and promising applications for surface modification and advanced nanomedicine. ACS Nano *13*, 8537–8565. https://doi.org/10.1021/acsnano.9b04436.

Choa, R., Tohyama, J., Wada, S., Meng, H., Hu, J., Okumura, M., May, R.M., Robertson, T.F., Pai, R.L., Nace, A., et al. (2021). Thymic stromal lymphopoietin induces adipose loss through sebum hypersecretion. Science *373*. https://doi.org/10.1126/science.abd2893.

Chouchani, E.T., Kazak, L., Jedrychowski, M.P., Lu, G.Z., Erickson, B.K., Szpyt, J., Pierce, K.A., Laznik-Bogoslavski, D., Vetrivelan, R., Clish, C.B., et al. (2016). Mitochondrial ROS regulate thermogenic energy expenditure and sulfenylation of UCP1. Nature *532*, 112–116. https://doi.org/10.1038/nature17399.

Chu, B., Zhong, R., Soncin, F., Stevenson, M.A., and Calderwood, S.K. (1998). Transcriptional activity of heat shock factor 1 at 37 degrees C is repressed through phosphorylation on two distinct serine residues by glycogen synthase kinase 3 and protein kinases Calpha and Czeta. J. Biol. Chem. *273*, 18640–18646. https://doi.org/10.1074/jbc.273.29.18640.

Chung, J., Nguyen, A.K., Henstridge, D.C., Holmes, A.G., Chan, M.H., Mesa, J.L., Lancaster, G.I., Southgate, R.J., Bruce, C.R., Duffy, S.J., et al. (2008). HSP72 protects against obesity-induced insulin resistance. Proc. Natl. Acad. Sci. USA *105*, 1739–1744. https://doi.org/10.1073/pnas.0705799105.

Cohen, P., Levy, J.D., Zhang, Y., Frontini, A., Kolodin, D.P., Svensson, K.J., Lo, J.C., Zeng, X., Ye, L., Khandekar, M.J., et al. (2014). Ablation of PRDM16 and beige adipose causes metabolic dysfunction and a subcutaneous to visceral fat switch. Cell *156*, 304–316. https://doi.org/10.1016/j.cell.2013.12.021.

Dai, C., and Sampson, S.B. (2016). HSF1: guardian of proteostasis in cancer. Trends Cell Biol. *26*, 17–28. https://doi.org/10.1016/j.tcb.2015.10.011.

Dong, B., Jaeger, A.M., and Thiele, D.J. (2019). Inhibiting heat shock factor 1 in cancer: a unique therapeutic opportunity. Trends Pharmacol. Sci. *40*, 986–1005. https://doi.org/10.1016/j.tips.2019.10.008.

Fu, Y.S., Wang, P.H., Liu, S.P., Huang, W.H., and Huang, H.T. (2010). Warm SPA-induced hyperthermia confers protection to rats against airway inflammation evoked by capsaicin and substance P. Auton. Neurosci. *155*, 49–58. https://doi.org/10.1016/j.autneu.2010.01.006.

Geissler, R., Simkin, A., Floss, D., Patel, R., Fogarty, E.A., Scheller, J., and Grimson, A. (2016). A widespread sequence-specific mRNA decay pathway mediated by hnRNPs A1 and A2/B1. Genes Dev. *30*, 1070–1085. https://doi.org/10.1101/gad.277392.116.

Gomez-Pastor, R., Burchfiel, E.T., Neef, D.W., Jaeger, A.M., Cabiscol, E., McKinstry, S.U., Doss, A., Aballay, A., Lo, D.C., Akimov, S.S., et al. (2017). Abnormal degradation of the neuronal stress-protective transcription factor HSF1 in Huntington's disease. Nat. Commun. *8*, 14405. https://doi.org/10.1038/ncomms14405.

Gomez-Pastor, R., Burchfiel, E.T., and Thiele, D.J. (2018). Regulation of heat shock transcription factors and their roles in physiology and disease. Nat. Rev. Mol. Cell Biol. *19*, 4–19. https://doi.org/10.1038/nrm.2017.73.

Harms, M., and Seale, P. (2013). Brown and beige fat: development, function and therapeutic potential. Nat. Med. *19*, 1252–1263. https://doi.org/10.1038/nm.3361.

Henriques, F., Bedard, A.H., Guilherme, A., Kelly, M., Chi, J., Zhang, P., Lifshitz, L.M., Bellvé, K., Rowland, L.A., Yenilmez, B., et al. (2020). Single-cell RNA profiling reveals adipocyte to macrophage signaling sufficient to enhance thermogenesis. Cell Rep. *32*, 107998. https://doi.org/10.1016/j.celrep.2020.107998.

Hoerter, J., Gonzalez-Barroso, M.D., Couplan, E., Mateo, P., Gelly, C., Cassard-Doulcier, A.M., Diolez, P., and Bouillaud, F. (2004). Mitochondrial uncoupling protein 1 expressed in the heart of transgenic mice protects against ischemic-reperfusion damage. Circulation *110*, 528–533. https://doi.org/10.1161/01.CIR.0000137824.30476.0E.

Holmberg, C.I., Hietakangas, V., Mikhailov, A., Rantanen, J.O., Kallio, M., Meinander, A., Hellman, J., Morrice, N., MacKintosh, C., Morimoto, R.I., et al. (2001). Phosphorylation of serine 230 promotes inducible transcriptional activity of heat shock factor 1. EMBO J. *20*, 3800–3810. https://doi.org/10.1093/emboj/20.14.3800.

Hooper, P.L. (1999). Hot-tub therapy for type 2 diabetes mellitus. N. Engl. J. Med. *341*, 924–925. https://doi.org/10.1056/NEJM199909163411216.

Ikeda, K., Kang, Q., Yoneshiro, T., Camporez, J.P., Maki, H., Homma, M., Shinoda, K., Chen, Y., Lu, X., Maretich, P., et al. (2017). UCP1-independent signaling involving SERCA2b-mediated calcium cycling regulates beige fat thermogenesis and systemic glucose homeostasis. Nat. Med. *23*, 1454–1465. https://doi.org/10.1038/nm.4429.

Jespersen, N.Z., Larsen, T.J., Peijs, L., Daugaard, S., Homøe, P., Loft, A., de Jong, J., Mathur, N., Cannon, B., Nedergaard, J., et al. (2013). A classical brown adipose tissue mRNA signature partly overlaps with brite in the supraclavicular region of adult humans. Cell Metab. *17*, 798–805. https://doi.org/10.1016/j.cmet.2013.04.011.

Ji, C., and Guo, X. (2019). The clinical potential of circulating microRNAs in obesity. Nat. Rev. Endocrinol. *15*, 731–743. https://doi.org/10.1038/s41574-019-0260-0.

Jimenez, V., Jambrina, C., Casana, E., Sacristan, V., Muñoz, S., Darriba, S., Rodó, J., Mallol, C., Garcia, M., León, X., et al. (2018). FGF21 gene therapy as treatment for obesity and insulin resistance. EMBO Mol. Med. *10*. https://doi.org/10.15252/emmm.201708791.

Jung, A.E., Fitzsimons, H.L., Bland, R.J., During, M.J., and Young, D. (2008). HSP70 and constitutively active HSF1 mediate protection against CDCrel-1-mediated toxicity. Mol. Ther. *16*, 1048–1055. https://doi.org/10.1038/mt.2008.68.

Kazak, L., Chouchani, E.T., Jedrychowski, M.P., Erickson, B.K., Shinoda, K., Cohen, P., Vetrivelan, R., Lu, G.Z., Laznik-Bogoslavski, D., Hasenfuss, S.C., et al. (2015). A creatine-driven substrate cycle enhances energy expenditure and thermogenesis in beige fat. Cell *163*, 643–655. https://doi.org/10.1016/j.cell.2015.09.035.

Kihara, T., Biro, S., Imamura, M., Yoshifuku, S., Takasaki, K., Ikeda, Y., Otuji, Y., Minagoe, S., Toyama, Y., and Tei, C. (2002). Repeated sauna treatment improves vascular endothelial and cardiac function in patients with chronic heart failure. J. Am. Coll. Cardiol. *39*, 754–759. https://doi.org/10.1016/s0735-1097(01)01824-1.

Kleiner, S., Mepani, R.J., Laznik, D., Ye, L., Jurczak, M.J., Jornayvaz, F.R., Estall, J.L., Chatterjee Bhowmick, D., Shulman, G.I., and Spiegelman, B.M. (2012). Development of insulin resistance in mice lacking PGC-1alpha in adipose tissues. Proc. Natl. Acad. Sci. USA *109*, 9635–9640. https://doi.org/10.1073/pnas.1207287109.

Kriszt, R., Arai, S., Itoh, H., Lee, M.H., Goralczyk, A.G., Ang, X.M., Cypess, A.M., White, A.P., Shamsi, F., Xue, R., et al. (2017). Optical visualisation of thermogenesis in stimulated single-cell brown adipocytes. Sci. Rep. *7*, 1383. https://doi.org/10.1038/s41598-017-00291-9.

Labbadia, J., Brielmann, R.M., Neto, M.F., Lin, Y.F., Haynes, C.M., and Morimoto, R.I. (2017). Mitochondrial stress restores the heat shock response and prevents proteostasis collapse during aging. Cell Rep. *21*, 1481–1494. https://doi.org/10.1016/j.celrep.2017.10.038.

Langmead, B., and Salzberg, S.L. (2012). Fast gapped-read alignment with Bowtie 2. Nat. Methods *9*, 357–359. https://doi.org/10.1038/nmeth.1923.

Larsen, T.M., Toubro, S., van Baak, M.A., Gottesdiener, K.M., Larson, P., Saris, W.H., and Astrup, A. (2002). Effect of a 28-d treatment with L-796568, a novel beta(3)-adrenergic receptor agonist, on energy expenditure and body composition in obese men. Am. J. Clin. Nutr. *76*, 780–788. https://doi.org/10.1093/ajcn/76.4.780.

Laukkanen, T., Khan, H., Zaccardi, F., and Laukkanen, J.A. (2015). Association between sauna bathing and fatal cardiovascular and all-cause mortality

events. JAMA Intern. Med. *175*, 542–548. https://doi.org/10.1001/jamainternmed.2014.8187.

Lin, C., Zhang, Y., Zhang, K., Zheng, Y., Lu, L., Chang, H., Yang, H., Yang, Y., Wan, Y., Wang, S., et al. (2019). Fever promotes T lymphocyte trafficking via a thermal sensory pathway involving heat shock protein 90 and α4 integrins. Immunity *50*, 137–151.e6. https://doi.org/10.1016/j.immuni.2018.11.013.

Liu, Y., Ai, K., and Lu, L. (2014). Polydopamine and its derivative materials: synthesis and promising applications in energy, environmental, and biomedical fields. Chem. Rev. *114*, 5057–5115. https://doi.org/10.1021/cr400407a.

Lo, K.A., Bauchmann, M.K., Baumann, A.P., Donahue, C.J., Thiede, M.A., Hayes, L.S., des Etages, S.A., and Fraenkel, E. (2011). Genome-wide profiling of H3K56 acetylation and transcription factor binding sites in human adipocytes. PLoS One *6*, e19778. https://doi.org/10.1371/journal.pone.0019778.

Long, J.Z., Svensson, K.J., Tsai, L., Zeng, X., Roh, H.C., Kong, X., Rao, R.R., Lou, J., Lokurkar, I., Baur, W., et al. (2014). A smooth muscle-like origin for beige adipocytes. Cell Metab. *19*, 810–820. https://doi.org/10.1016/j.cmet.2014.03.025.

Lute, B., Jou, W., Lateef, D.M., Goldgof, M., Xiao, C., Piñol, R.A., Kravitz, A.V., Miller, N.R., Huang, Y.G., Girardet, C., et al. (2014). Biphasic effect of melanocortin agonists on metabolic rate and body temperature. Cell Metab. *20*, 333–345. https://doi.org/10.1016/j.cmet.2014.05.021.

Ma, X., Xu, L., Alberobello, A.T., Gavrilova, O., Bagattin, A., Skarulis, M., Liu, J., Finkel, T., and Mueller, E. (2015). Celastrol protects against obesity and metabolic dysfunction through activation of a HSF1-PGC1alpha transcriptional axis. Cell Metab. *22*, 695–708. https://doi.org/10.1016/j.cmet.2015.08.005.

Martinez, F.J., Pratt, G.A., Van Nostrand, E.L., Batra, R., Huelga, S.C., Kapeli, K., Freese, P., Chun, S.J., Ling, K., Gelboin-Burkhart, C., et al. (2016). Protein-RNA networks regulated by normal and ALS-associated mutant HNRNPA2B1 in the nervous system. Neuron *92*, 780–795. https://doi.org/10.1016/j.neuron.2016.09.050.

Masuda, Y., Marui, S., Kato, I., Fujiki, M., Nakada, M., and Nagashima, K. (2019). Thermal and cardiovascular responses and thermal sensation during hot-water bathing and the influence of room temperature. J. Therm. Biol. *82*, 83–89. https://doi.org/10.1016/j.jtherbio.2019.03.014.

Mendillo, M.L., Santagata, S., Koeva, M., Bell, G.W., Hu, R., Tamimi, R.M., Fraenkel, E., Ince, T.A., Whitesell, L., and Lindquist, S. (2012). HSF1 drives a transcriptional program distinct from heat shock to support highly malignant human cancers. Cell *150*, 549–562. https://doi.org/10.1016/j.cell.2012.06.031.

Mina, A.I., LeClair, R.A., LeClair, K.B., Cohen, D.E., Lantier, L., and Banks, A.S. (2018). CalR: a web-based analysis tool for indirect calorimetry experiments. Cell Metab. *28*, 656–666.e1. https://doi.org/10.1016/j.cmet.2018.06.019.

Nedergaard, J., Bengtsson, T., and Cannon, B. (2007). Unexpected evidence for active brown adipose tissue in adult humans. Am. J. Physiol. Endocrinol. Metab. *293*, E444–E452. https://doi.org/10.1152/ajpendo.00691.2006.

Neudegger, T., Verghese, J., Hayer-Hartl, M., Hartl, F.U., and Bracher, A. (2016). Structure of human heat-shock transcription factor 1 in complex with DNA. Nat. Struct. Mol. Biol. *23*, 140–146. https://doi.org/10.1038/nsmb.3149.

Nguyen, H.P., Yi, D., Lin, F., Viscarra, J.A., Tabuchi, C., Ngo, K., Shin, G., Lee, A.Y., Wang, Y., and Sul, H.S. (2020). Aifm2, a NADH oxidase, supports robust glycolysis and is required for cold- and diet-induced thermogenesis. Mol. Cell *77*, 600–617.e4. https://doi.org/10.1016/j.molcel.2019.12.002.

Nguyen, K.D., Qiu, Y., Cui, X., Goh, Y.P., Mwangi, J., David, T., Mukundan, L., Brombacher, F., Locksley, R.M., and Chawla, A. (2011). Alternatively activated macrophages produce catecholamines to sustain adaptive thermogenesis. Nature *480*, 104–108. https://doi.org/10.1038/nature10653.

O'Sullivan, D., Stanczak, M.A., Villa, M., Uhl, F.M., Corrado, M., Klein Geltink, R.I., Sanin, D.E., Apostolova, P., Rana, N., Edwards-Hicks, J., et al. (2021). Fever supports $CD8^+$ effector T cell responses by promoting mitochondrial translation. Proc. Natl. Acad. Sci. USA *118*. e2023752118. https://doi.org/10.1073/pnas.2023752118.

Patsouris, D., Qi, P., Abdullahi, A., Stanojcic, M., Chen, P., Parousis, A., Amini-Nik, S., and Jeschke, M.G. (2015). Burn induces browning of the subcutaneous white adipose tissue in mice and humans. Cell Rep. *13*, 1538–1544. https://doi.org/10.1016/j.celrep.2015.10.028.

Pellegrinelli, V., Peirce, V.J., Howard, L., Virtue, S., Türei, D., Senzacqua, M., Frontini, A., Dalley, J.W., Horton, A.R., Bidault, G., et al. (2018). Adipocyte-secreted BMP8b mediates adrenergic-induced remodeling of the neurovascular network in adipose tissue. Nat. Commun. *9*, 4974. https://doi.org/10.1038/s41467-018-07453-x.

Purcell, S., Neale, B., Todd-Brown, K., Thomas, L., Ferreira, M.A., Bender, D., Maller, J., Sklar, P., de Bakker, P.I., Daly, M.J., and Sham, P.C. (2007). PLINK: a tool set for whole-genome association and population-based linkage analyses. Am. J. Hum. Genet. *81*, 559–575. https://doi.org/10.1086/519795.

Qiao, A., Jin, X., Pang, J., Moskophidis, D., and Mivechi, N.F. (2017). The transcriptional regulator of the chaperone response HSF1 controls hepatic bioenergetics and protein homeostasis. J. Cell Biol. *216*, 723–741. https://doi.org/10.1083/jcb.201607091.

Redman, L.M., de Jonge, L., Fang, X., Gamlin, B., Recker, D., Greenway, F.L., Smith, S.R., and Ravussin, E. (2007). Lack of an effect of a novel beta3-adrenoceptor agonist, TAK-677, on energy metabolism in obese individuals: a double-blind, placebo-controlled randomized study. J. Clin. Endocrinol. Metab. *92*, 527–531. https://doi.org/10.1210/jc.2006-1740.

Robinson, J.T., Thorvaldsdóttir, H., Winckler, W., Guttman, M., Lander, E.S., Getz, G., and Mesirov, J.P. (2011). Integrative genomics viewer. Nat. Biotechnol. *29*, 24–26. https://doi.org/10.1038/nbt.1754.

Rosen, E.D., and Spiegelman, B.M. (2014). What we talk about when we talk about fat. Cell *156*, 20–44. https://doi.org/10.1016/j.cell.2013.12.012.

Scheja, L., and Heeren, J. (2019). The endocrine function of adipose tissues in health and cardiometabolic disease. Nat. Rev. Endocrinol. *15*, 507–524. https://doi.org/10.1038/s41574-019-0230-6.

Seki, T., Hosaka, K., Fischer, C., Lim, S., Andersson, P., Abe, M., Iwamoto, H., Gao, Y., Wang, X., Fong, G.H., and Cao, Y. (2018). Ablation of endothelial VEGFR1 improves metabolic dysfunction by inducing adipose tissue browning. J. Exp. Med. *215*, 611–626. https://doi.org/10.1084/jem.20171012.

Shiuchi, T., Haque, M.S., Okamoto, S., Inoue, T., Kageyama, H., Lee, S., Toda, C., Suzuki, A., Bachman, E.S., Kim, Y.B., et al. (2009). Hypothalamic orexin stimulates feeding-associated glucose utilization in skeletal muscle via sympathetic nervous system. Cell Metab. *10*, 466–480. https://doi.org/10.1016/j.cmet.2009.09.013.

Soncin, F., Zhang, X., Chu, B., Wang, X., Asea, A., Ann Stevenson, M., Sacks, D.B., and Calderwood, S.K. (2003). Transcriptional activity and DNA binding of heat shock factor-1 involve phosphorylation on threonine 142 by CK2. Biochem. Biophys. Res. Commun. *303*, 700–706. https://doi.org/10.1016/s0006-291x(03)00398-x.

St-Pierre, J., Drori, S., Uldry, M., Silvaggi, J.M., Rhee, J., Jäger, S., Handschin, C., Zheng, K., Lin, J., Yang, W., et al. (2006). Suppression of reactive oxygen species and neurodegeneration by the PGC-1 transcriptional coactivators. Cell *127*, 397–408. https://doi.org/10.1016/j.cell.2006.09.024.

Sveidahl Johansen, O., Ma, T., Hansen, J.B., Markussen, L.K., Schreiber, R., Reverte-Salisa, L., Dong, H., Christensen, D.P., Sun, W., Gnad, T., et al. (2021). Lipolysis drives expression of the constitutively active receptor GPR3 to induce adipose thermogenesis. Cell *184*, 3502–3518.e33. https://doi.org/10.1016/j.cell.2021.04.037.

Symonds, M.E., Henderson, K., Elvidge, L., Bosman, C., Sharkey, D., Perkins, A.C., and Budge, H. (2012). Thermal imaging to assess age-related changes of skin temperature within the supraclavicular region co-locating with brown adipose tissue in healthy children. J. Pediatr. *161*, 892–898. https://doi.org/10.1016/j.jpeds.2012.04.056.

Tharp, K.M., Higuchi-Sanabria, R., Timblin, G.A., Ford, B., Garzon-Coral, C., Schneider, C., Muncie, J.M., Stashko, C., Daniele, J.R., Moore, A.S., et al. (2021). Adhesion-mediated mechanosignaling forces mitohormesis. Cell Metab. *33*, 1322–1341.e13. https://doi.org/10.1016/j.cmet.2021.04.017.

Thomas, K.N., van Rij, A.M., Lucas, S.J., and Cotter, J.D. (2017). Lower-limb hot-water immersion acutely induces beneficial hemodynamic and cardiovascular responses in peripheral arterial disease and healthy, elderly controls. Am.

J. Physiol. Regul. Integr. Comp. Physiol. *312*, R281–R291. https://doi.org/10.1152/ajpregu.00404.2016.

Tschöp, M.H., Speakman, J.R., Arch, J.R., Auwerx, J., Brüning, J.C., Chan, L., Eckel, R.H., Farese, R.V., Jr., Galgani, J.E., Hambly, C., et al. (2011). A guide to analysis of mouse energy metabolism. Nat. Methods *9*, 57–63. https://doi.org/10.1038/nmeth.1806.

Uchiyama, T., Atsuta, H., Utsugi, T., Oguri, M., Hasegawa, A., Nakamura, T., Nakai, A., Nakata, M., Maruyama, I., Tomura, H., et al. (2007). HSF1 and constitutively active HSF1 improve vascular endothelial function (heat shock proteins improve vascular endothelial function). Atherosclerosis *190*, 321–329. https://doi.org/10.1016/j.atherosclerosis.2006.03.037.

van Marken Lichtenbelt, W.D., Vanhommerig, J.W., Smulders, N.M., Drossaerts, J.M., Kemerink, G.J., Bouvy, N.D., Schrauwen, P., and Teule, G.J. (2009). Cold-activated brown adipose tissue in healthy men. N. Engl. J. Med. *360*, 1500–1508. https://doi.org/10.1056/NEJMoa0808718.

Vasconcelos, J., Freire, E., Almendra, R., Silva, G.L., and Santana, P. (2013). The impact of winter cold weather on acute myocardial infarctions in Portugal. Environ. Pollut. *183*, 14–18. https://doi.org/10.1016/j.envpol.2013.01.037.

Vinaik, R., Barayan, D., Abdullahi, A., and Jeschke, M.G. (2019). NLRP3 inflammasome mediates white adipose tissue browning after burn. Am. J. Physiol. Endocrinol. Metab. *317*, E751–E759. https://doi.org/10.1152/ajpendo.00180.2019.

Virtanen, K.A., Lidell, M.E., Orava, J., Heglind, M., Westergren, R., Niemi, T., Taittonen, M., Laine, J., Savisto, N.J., Enerbäck, S., and Nuutila, P. (2009). Functional brown adipose tissue in healthy adults. N. Engl. J. Med. *360*, 1518–1525. https://doi.org/10.1056/NEJMoa0808949.

Vitali, A., Murano, I., Zingaretti, M.C., Frontini, A., Ricquier, D., and Cinti, S. (2012). The adipose organ of obesity-prone C57BL/6J mice is composed of mixed white and brown adipocytes. J. Lipid Res. *53*, 619–629. https://doi.org/10.1194/jlr.M018846.

Wang, L., Wen, M., and Cao, X. (2019). Nuclear hnRNPA2B1 initiates and amplifies the innate immune response to DNA viruses. Science *365*, eaav0758. https://doi.org/10.1126/science.aav0758.

Wang, T., Ma, X., Peng, D., Zhang, R., Sun, X., Chen, M., Yan, J., Wang, S., Yan, D., He, Z., et al. (2016a). Effects of obesity related genetic variations on visceral and subcutaneous fat distribution in a Chinese population. Sci. Rep. *6*, 20691. https://doi.org/10.1038/srep20691.

Wang, X., Ni, L., Wan, S., Zhao, X., Ding, X., Dejean, A., and Dong, C. (2020). Febrile temperature critically controls the differentiation and pathogenicity of T helper 17 cells. Immunity *52*, 328–341.e5. https://doi.org/10.1016/j.immuni.2020.01.006.

Wang, X., Wang, C.P., Wang, X.Y., Wang, Y.T., Zhang, Q., and Cheng, Y.Y. (2017). A polydopamine nanoparticle-knotted poly(ethylene glycol) hydrogel for on-demand drug delivery and chemo-photothermal therapy. Chem. Mater. *29*, 1370–1376. https://doi.org/10.1021/acs.chemmater.6b05192.

Wang, X., Zhang, J., Wang, Y., Wang, C., Xiao, J., Zhang, Q., and Cheng, Y. (2016b). Multi-responsive photothermal-chemotherapy with drug-loaded melanin-like nanoparticles for synergetic tumor ablation. Biomaterials *81*, 114–124. https://doi.org/10.1016/j.biomaterials.2015.11.037.

Westerheide, S.D., Bosman, J.D., Mbadugha, B.N., Kawahara, T.L., Matsumoto, G., Kim, S., Gu, W., Devlin, J.P., Silverman, R.B., and Morimoto, R.I. (2004). Celastrols as inducers of the heat shock response and cytoprotection. J. Biol. Chem. *279*, 56053–56060. https://doi.org/10.1074/jbc.M409267200.

Wu, J., Boström, P., Sparks, L.M., Ye, L., Choi, J.H., Giang, A.H., Khandekar, M., Virtanen, K.A., Nuutila, P., Schaart, G., et al. (2012). Beige adipocytes are a distinct type of thermogenic fat cell in mouse and human. Cell *150*, 366–376. https://doi.org/10.1016/j.cell.2012.05.016.

Xu, L., Ma, X., Bagattin, A., and Mueller, E. (2016). The transcriptional coactivator PGC1α protects against hyperthermic stress via cooperation with the heat shock factor HSF1. Cell Death Dis. *7*, e2102. https://doi.org/10.1038/cddis.2016.22.

Xu, Y., Ma, X., Shen, Y., Gu, C., Tang, J., and Bao, Y. (2019). Role of hyperglycaemia in the relationship between serum osteocalcin levels and relative skeletal muscle index. Clin. Nutr. *38*, 2704–2711. https://doi.org/10.1016/j.clnu.2018.11.025.

Ye, L., Wu, J., Cohen, P., Kazak, L., Khandekar, M.J., Jedrychowski, M.P., Zeng, X., Gygi, S.P., and Spiegelman, B.M. (2013). Fat cells directly sense temperature to activate thermogenesis. Proc. Natl. Acad. Sci. USA *110*, 12480–12485. https://doi.org/10.1073/pnas.1310261110.

Yu, G., Wang, L.G., Han, Y., and He, Q.Y. (2012). clusterProfiler: an R package for comparing biological themes among gene clusters. Omics *16*, 284–287. https://doi.org/10.1089/omi.2011.0118.

Yu, T., Dohl, J., Chen, Y., Gasier, H.G., and Deuster, P.A. (2019). Astaxanthin but not quercetin preserves mitochondrial integrity and function, ameliorates oxidative stress, and reduces heat-induced skeletal muscle injury. J. Cell. Physiol. *234*, 13292–13302. https://doi.org/10.1002/jcp.28006.

Yun, J., and Finkel, T. (2014). Mitohormesis. Cell Metab. *19*, 757–766. https://doi.org/10.1016/j.cmet.2014.01.011.

Zeng, X., Ye, M., Resch, J.M., Jedrychowski, M.P., Hu, B., Lowell, B.B., Ginty, D.D., and Spiegelman, B.M. (2019). Innervation of thermogenic adipose tissue via a calsyntenin 3beta-S100b axis. Nature *569*, 229–235. https://doi.org/10.1038/s41586-019-1156-9.

Zhang, Y., Liu, T., Meyer, C.A., Eeckhoute, J., Johnson, D.S., Bernstein, B.E., Nusbaum, C., Myers, R.M., Brown, M., Li, W., and Liu, X.S. (2008). Model-based analysis of ChIP-Seq (MACS). Genome Biol. *9*, R137. https://doi.org/10.1186/gb-2008-9-9-r137.

Zhang, Z., Funcke, J.B., Zi, Z., Zhao, S., Straub, L.G., Zhu, Y., Zhu, Q., Crewe, C., An, Y.A., Chen, S., et al. (2021). Adipocyte iron levels impinge on a fat-gut crosstalk to regulate intestinal lipid absorption and mediate protection from obesity. Cell Metab *33*, 1624–1639.e9. https://doi.org/10.1016/j.cmet.2021.06.001.

Zhou, Z., Yan, Y., Hu, K., Zou, Y., Li, Y., Ma, R., Zhang, Q., and Cheng, Y. (2017). Autophagy inhibition enabled efficient photothermal therapy at a mild temperature. Biomaterials *141*, 116–124. https://doi.org/10.1016/j.biomaterials.2017.06.030.

STAR★METHODS

KEY RESOURCES TABLE

REAGENT or RESOURCE	SOURCE	IDENTIFIER
Antibodies		
Rabbit-anti-HSF1 antibody	CST	Cat# 4356S; RRID: AB_10695463
Mouse-anti-PGC1α antibody	Santa Cruz	Cat# sc-517380; RRID: AB_2755043
Rabbit-anti-UCP1 antibody	Abcam	Cat# ab10983; RRID: AB_2241462
Mouse-anti-β-ACTIN antibody	Sigma-Aldrich	Cat# A3854; RRID: AB_262011
Rabbit-anti-HNRNPA2B1 antibody	Abcam	Cat# ab31645; RRID: AB_732978
Normal Rabbit IgG Antibody	CST	Cat# 2729; RRID: AB_1031062
IRDye 680RD Goat anti-Rabbit IgG (H +L) Secondary Antibody	LI-COR	Cat# 926-68071; RRID: AB_10956166
IRDye 800CW goat anti-mouse IgG (H+L) Secondary Antibody	LI-COR	Cat# 926-32210; RRID: AB_621842
Mouse anti-HSF1 antibody	Santa Cruz	Cat# sc-17757; RRID: AB_627753
Goat anti-rabbit Alexa 488	Thermo Fisher	Cat# A11034; RRID: AB_2576217
Goat anti-mouse Alexa 594	Thermo Fisher	Cat# A11032; RRID: AB_2534091
Bacterial and virus strains		
Adenovirus:Hnrnpa2b1	This paper	N/A
Adeno-associated virus: HSF1 active form	This paper	N/A
Lentivirus: HSF1 wild-type (CC)	This paper	N/A
Lentivirus: HSF1 Pro365Thr variant (AA)	This paper	N/A
Adeno-associated virus: Hnrnpa2b1	This paper	N/A
Adeno-associated virus: HSF1 shRNA	This paper	N/A
Adeno-associated virus: Hnrnpa2b1 shRNA	This paper	N/A
Chemicals, peptides, and recombinant proteins		
PDA-PEG hydrogel	(Wang et al., 2017)	N/A
RNAiso Plus	Takara	Cat# 9108
PrimeScript™RT Master Mix	Takara	Cat# RR036A
Hieff® qPCR SYBR Green Master Mix (Low Rox Plus)	Yeasen	Cat# 11202ES03
DMEM, high glucose, with L-glutamine	Gibco	Cat# 11995065
Fetal Bovine Serum	Gibco	Cat# 10270
Forskolin	Sigma-Aldrich	Cat# F6886
CL 316,243	Sigma-Aldrich	Cat# 5976
Dexamethasone	Sigma-Aldrich	Cat# D4902
Insulin solution	Sigma-Aldrich	Cat# I9278
Indomethacin	Sigma-Aldrich	Cat# I8280
3-Isobutyl-1-methylxanthine (IBMX)	Sigma-Aldrich	Cat# I5879
Lipofectamine2000 Transfection Reagent	Thermo Fisher	Cat# 11668030
Oil Red O	Sigma-Aldrich	Cat# O0625
Formalin solution, neutral buffered, 10%	Sigma-Aldrich	Cat# HT501128-4L
RIPA Lysis and Extraction Buffer	Thermo Fisher	Cat# 89900
Phenyl methane sulfonyl fluoride (PMSF)	Thermo Fisher	Cat# 36978
Protease inhibitors	Thermo Fisher	Cat# A32963
Rosiglitazone	Sigma-Aldrich	Cat# R2408
T3 (3,3',5-Triiodo-L-thyronine)	Sigma-Aldrich	Cat# T2877
D-glucose	Sigma-Aldrich	Cat# GT528

(*Continued on next page*)

Continued

REAGENT or RESOURCE	SOURCE	IDENTIFIER
Penicillin-Streptomycin	Gibco	Cat# 15070063
Actinomycin D	Sigma-Aldrich	Cat# SBR00013
Clodronate-loaded liposomes	Liposoma	Cat# CP-005-005
Hematoxylin and eosin	Beyotime	Cat# C0105S
EZ-Trans transfection kit	Life Ilab Biotechnology	Cat# C4058L1090
ErthermAC	Emdmillipore	Cat# SCT057
Cell Counting Kit-8	Beyotime	Cat# C0041
α-methyl-p-tyrosine (α-MT)	Sigma-Aldrich	Cat# M3281
Benzoic acid	Parr Instrument Company	Cat# 3413
Critical commercial assays		
Triglyceride quantification kit	BioVision	Cat# K622
Total Cholesterol quantification kit	Sigma-Aldrich	Cat# MAK043
HDL/LDL quantification kit	Sigma-Aldrich	Cat# MAK045
AST activity assay kit	Sigma-Aldrich	Cat# MAK055
ALT activity assay kit	Sigma-Aldrich	Cat# MAK052
Creatine Kinase (CK) activity assay kit	Sigma-Aldrich	Cat# MAK116
Uric Acid assay kit	Sigma-Aldrich	Cat# MAK077
Creatinine assay kit	Sigma-Aldrich	Cat# MAK080
Urea nitrogen assay kit	Sigma-Aldrich	Cat# MAK006
Albumin assay kit	Sigma-Aldrich	Cat# 09753
Total protein assay kit	Sigma-Aldrich	Cat# 71285-M
Alkaline phosphatase activity assay kit	Abcam	Cat# ab83369
Amylase activity assay kit	Sigma-Aldrich	Cat# MAK009
Lactate dehydrogenase activity assay kit	Sigma-Aldrich	Cat# MAK066
Mouse Noradrenaline, NA ELISA Kit	CUSABIO	Cat# CSB-E07870m
Human Noradrenaline Research ELISA kits	LDN	Cat# BA E-5200
QIAamp DNA Blood Mini Kit	QIAGEN	Cat# 51106
Mouse Cortisol ELISA Kit	CUSABIO	Cat# CSB-E05113m
SimpleChIP® Enzymatic Chromatin IP Kit (Magnetic Beads)	CST	Cat# 9003
Magna RIP™ RNA-Binding Protein Immunoprecipitation Kit	Millpore	Cat# 17-700
Dual luciferase reporter assay kit	Promega	Cat# E1960
BCA protein assay kit	Beyotime	Cat# P0012
Deposited data		
ChIP-seq data in mice beige adipocytes	This paper	GSE176375
ChIP-seq data in human adipocytes differentiated from mesenchymal stem cells	(Lo et al., 2011)	GSE24326
RNA-seq data	This paper	GSE176376
Raw and analyzed data: genotype data from Nicheng Cohort and FADE cohort	This paper	NODE: OEP003133 http://www.biosino.org/node/project/detail/OEP003133
Experimental models: Cell lines		
HEK293T cell	ATCC	Cat# CRL-3216; RRID: CVCL_0063
C3H10T1/2 cell	ATCC	Cat# CCL-226; RRID: CVCL_0190
Immortalized beige preadipocytes line	This paper	N/A
Immortalized brown preadipocytes line	This paper	N/A
Primary beige preadipocytes	This paper	N/A

(*Continued on next page*)

Continued

REAGENT or RESOURCE	SOURCE	IDENTIFIER
Experimental models: Organisms/strains		
Mouse: C57BL/6J	Jackson Laboratories	Cat# JAX 000664; RRID: IMSR_JAX:000664
Mouse: *Adiponectin-Cre*	Jackson Laboratories	Cat# JAX 028020; RRID: IMSR_JAX:028020
Mouse: *Adiponectin-Cre Hsf1*$^{loxp/loxp}$	This paper	N/A
Mouse: *Hnrnpa2b1* heterozygous	This paper	N/A
Oligonucleotides		
Primers for qPCRs, sequence provided in Table S4	This paper	N/A
Primers for ChIP qPCRs, sequence provided in Table S4	This paper	N/A
Recombinant DNA		
Plasmid: pcDNA3.1	Invitrogen	Cat# V795-20
Plasmid: PCDH-HSF1 wild-type (CC) and Pro365Thr variant (AA)	This paper	N/A
Plasmid: PGL4.17-A2B1 promoter (WT and A2b1 mHSE)	This paper	N/A
pMD2.G	Addgene	Cat# 12259
psPAX2	Addgene	Cat# 12260
Software and algorithms		
GraphPad Prism V7	GraphPad Software	https://www.graphpad.com/
FLIR Tools	FLIR System	http://support.flir.com
FlowJo	FlowJo	http://www.flowjo.com/
FastQC	(Andrews, 2010)	http://www.bioinformatics.babraham.ac.uk/projects/fastqc/
Bowtie2 (v.2.2.5)	(Langmead and Salzberg, 2012)	http://bowtie-bio.sourceforge.net/bowtie2/index.shtml;
MACS2 (v2.1.1)	(Zhang et al., 2008)	https://github.com/taoliu/MACS
Integrative Genomic Viewer genome (IGV) browser (v.2.8.0)	(Robinson et al., 2011)	https://software.broadinstitute.org/software/igv/
Moor LDI Image Processing software	Moor Instruments	https://www.moor.co.uk/products/control/moorldi2-research-software/
SPSS Statistics 23	IBM	N/A
PLINK	(Purcell et al., 2007)	http://zzz.bwh.harvard.edu/plink/
Other		
High Fat Diet	Research Diets	Cat# D12492
808-nm near-infrared (NIR) laser	Changchun New Industries Optoelectronics Technology Co.	N/A
infrared camera FLIR E60	FLIR Systems AB	N/A
AccuFat-1050	Mag-med	N/A
Metabolic Chamber-Comprehensive Lab Animal Monitoring System (CLAMS)	Columbus Instruments	N/A
Roche LightCycler480	Roche	N/A
Nanodrop spectrophotometer	Thermo Fisher	N/A
Optical microscope	Nikon	N/A
High-resolution Laser-Doppler Imaging (HR-LDI)	Moor Instruments	N/A
Temperature-controlled incubator	NK system	N/A

(*Continued on next page*)

Continued

REAGENT or RESOURCE	SOURCE	IDENTIFIER
Infrared thermal imaging camera	Magnity Electronics	N/A
Rectal thermometer TH-5	Braintree	N/A
DHG-9240A High Temperature Drying Oven	Shanghai Jinghong Corporation	N/A
6400 Automatic Isoperibol Calorimeter	Parr Instrument Company	N/A

RESOURCE AVAILABILITY

Lead contact

Further information and requests for resources and reagents should be directed to and will be fulfilled by the Lead contact, Professor Xinran Ma (xrma@bio.ecnu.edu.cn).

Materials availability

All mouse lines and plasmids generated in this study are available from the Lead Contact with a completed Materials Transfer Agreement.

Data and code availability

The ChIP-seq and RNA-seq datasets generated during this study are accessible at GEO: GSE176375, GSE176376. The human genotype data for genetic variants in *HSF1* gene region can be found in the National Omics Data Encyclopedia (NODE) with accession number OEP003133 (http://www.biosino.org/node/project/detail/OEP003133). Individual phenotype data cannot be shared due to informed consent regulations.

This paper does not report original code.

Any additional information required to reanalyze the data reported in this paper is available from the lead contact upon request.

EXPERIMENTAL MODEL AND SUBJECT DETAILS

Animals

All animal experiments were performed in accordance with procedures approved by the ethics committee of Animal experiments of East China Normal University. Mice were allocated to experimental groups randomly. 8-week male C57BL/6J mice were used in the study. Mice with a targeted deletion of HSF1 in adipose tissues (Adiponectin-Cre $Hsf1^{loxp/loxp}$) were generated by crossing the $Hsf1^{loxp/loxp}$ mice with transgenic mice expressing Cre-recombinase under the control of the adiponectin promoter (Adiponectin-Cre). Littermates expressing no Cre (WT mice) were used as a control group throughout the experiments. Hnrnpa2b1 heterozygous mice were generated by Shanghai Bioray Laboratory with single strand exon 2-6 deletion. Mice were kept at 22°C at room temperature under a 12-hour light/dark cycle with free access to food and water. For thermoneutral environment, mice were kept at 30°C in a temperature-controlled chamber (LP-80LED-6CTAR, NK system).

Local hyperthermia therapy in mice

8-week-old mice were injected with PDA/PEG hydrogel (PDA) (Wang et al., 2016b) bilaterally in inguinal fat pads (iWAT) and the skin areas covering beige fat were illuminated with an 808-nm near-infrared (NIR) laser for 10 minutes (LHT) for each session, while the other group underwent the same protocol but without NIR illumination (Sham). The NIR intensity and iWAT loci temperature were closely monitored during the whole illumination period to ensure a local hyperthermia of 41±0.5°C in the inguinal area. The temperature was raised to indicated degrees within 0.5 minutes and maintained for 10 minutes. Core temperatures were monitored during the experimental process with a rectal thermometer (Braintree, TH-5) and skin temperatures were recorded with an infrared thermal imaging camera (Magnity Electronics). Mice were returned to normal housing environment at 22°C after treatment. For chronic LHT, LHT group were treated with illumination for 10 minutes while Sham group were sham treated once every three days. For acute experiment, mice were treated with illumination unilaterally on one side of iWAT (LHT) for 10 minutes while the other side of iWAT remained unilluminated (Sham). Images were taken with an infrared camera (FLIR E60, FLIR Systems) or tissue samples were collected after 24 hours.

For LHT on BAT, mice were anesthetized with isoflurane during the whole operation, and the incision site was shaved and disinfected using 70% ethanol. A longitudinal incision at the interscapular region was performed to expose the brown fat as previously reported (Sveidahl Johansen et al., 2021). PDA was bilaterally injected into both lobes of the brown fat and the incisions were sutured after injection. After surgery, all mice received carprofen (5 mg/kg) by intraperitoneal injection. Animals were received carprofen (5mg/kg) and monitored daily till the wound healing. LHT group were then treated with illumination at interscapular region at 41±0.5°C for 10 min while Sham group were sham treated.

Local delivery of adeno-associated virus (AAV) in adipose tissues

Adeno-associated virus (AAV) vector-mediated overexpression of mouse Hsf1 active form, Hnrnpa2b1, control (GFP), shRNA targeting Hnrnpa2b1 and scrambled control (GFP) were constructed, amplified, and purified by Hanbio biotechnology (Shanghai, China). A total of 50 μl of $1*10^9$ Vg/μl of each AAV diluted in PBS was injected into the inguinal fat pads of mice (Jimenez et al., 2018). Mice were monitored for changes in body weight, fat mass, cold tolerance, and oxygen consumption, then mice were sacrificed and tissues were dissected for further analysis.

Macrophage depletion in adipose tissues

In prior to macrophage depletion, 8-weeks old mice were injected with PDA/PEG hydrogel (PDA) bilaterally in inguinal fat pads. Two days later, these mice were injected with 110mg/kg of clodronate-loaded liposomes (Liposoma, CP-005-005) every two days for three times. Afterwards, skin areas covering beige fat were illuminated unilaterally on one side of iWAT with an 808-nm near-infrared (NIR) laser for 10 min (LHT) while the other side of iWAT remained unilluminated (Sham). Mice were sacrificed to collect iWAT tissues for further analysis after 24 h.

Local hyperthermia therapy in human subjects

The study was conducted according to the ethical guidelines of the East China Normal University and all the subjects have signed informed consent to participate in the study (HR 042-2021). The study involved 33 healthy individuals (17 males, 16 females) with ages of 24.6 (SD±1.8) years and with normal BMI of 22.01 (SD±3.53) kg/m^2. The subjects were requested to follow a similar daily schedule, including time and composition of meals, rest/active hours and amounts of exercises, and avoid vigorous exercise, caffeine, drugs or alcohol consumption one week prior to the experiment to avoid impacts of circadian rhythm/life style on thermogenesis. For local hyperthermia therapy, each subject was in a relaxed state within a familiar, temperature- and humidity-controlled room, where they were seated in an upright posture, with arms adducted and wearing a standard test robe with head, neck, and shoulders unclothed and one meter away from a thermal imaging camera (FLIR E60, FLIR Systems) fixed on a tripod to ensure visualization of the supraclavicular depots. The test room was kept quiet and strictly undisturbed while all volunteers were instructed to maintain a relax posture with minimal movement during the whole test procedure to avoid unnecessary influences on body heat production. Participants were acclimated in the test room for one h prior to baseline imaging. After baseline imaging, the supraclavicular fat depots (around upper shoulder/upper back area) of participants were exposed to a thermal source (41±0.5°C) for 20 min. After thermal source removal, subjects were rested for 2 h and thermal images of their supraclavicular depots were taken and analyzed. Human core temperatures and skin temperatures were monitored before and after LHT. Afterwards, the exact same experimental protocols were repeated but without thermal source application on every volunteer as Sham. Serum NE levels were examined in 20 healthy individuals (10 males, 10 females) among these subjects after Sham or LHT treatment with Noradrenaline ELISA kits (LDN, BA E-5200) according to the manufacturer's instructions. These same 20 individuals were subjected to long-term LHT on Monday, Wednesday and Friday each week for 5 weeks and parameters were collected following same protocols mentioned above.

Human participants for genotyping

10082 subjects from Shanghai FAt Distribution and disease (FADE) cohort and Nicheng cohort (Bao et al., 2013; Chen et al., 2018; Wang et al., 2016a; Xu et al., 2019) were included for human HSF1 genotyping analysis. Detailed standard about recruitment and clinical data acquisition were described previously (Bao et al., 2013; Chen et al., 2018; Wang et al., 2016a; Xu et al., 2019), and subjects with diabetes were excluded. Human study was approved by Shanghai Jiaotong University Affiliated Sixth People's Hospital according to Declaration of Helsinki II. Written informed consent was obtained from all subjects. The metabolic traits of human participants were summarized in Table S3.

Genomic DNA was extracted from blood samples by QIAamp DNA Blood Mini Kit (, Hilden, Germany). Genotyping was performed by Infinium Asian Screening Array, Multi-Ethnic Genotyping Array and Infinium Exome array platform. Single nucleotide polymorphisms (SNPs) passed through quality-control procedure were further analyzed (call rate ≥98%, concordant rate ≥99% and Hardy Weinberg equilibrium was approved (P>0.01). As for participants, all subjects had call rate ≥95%. Imputation was conducted according to 504 East-Asian subjects from 1000 Genomes Project phase III, SNPs with rsq value ≥0.4 were retained. SNPs from different genotyping array were analyzed together after imputation. rs78202224 was genotyped in all subjects.

The statistical analysis was performed by PLINK (Purcell et al., 2007) and SAS (version 9.2, SAS Institute, Cary, NC). Descriptive statistics were shown by different rs78202224 genotype groups. Quantitative traits with skewed distribution were logarithmically transformed. Multiple linear regression was performed after adjusting for age and sex as confounding factors.

Differentiated adipocytes

C3H10T1/2 (ATCC) cells were maintained in Dulbecco's Modified Eagle Medium (DMEM, Gibco, 11995065) supplemented with 10% fetal bovine serum (FBS, Gibco, 10270) and 1% penicillin and streptomycin (Gibco, 15070063) in a humidified incubator at 37°C with 5% CO_2. Primary preadipocytes, immortalized beige and brown preadipocytes were maintained in DMEM supplemented with 20% fetal bovine serum and 1% penicillin and streptomycin.

For differentiation procedure, C3H10T1/2 cells were induced to differentiate to beige/brown adipocytes in differentiation medium supplemented with 5μg/ml insulin (Sigma-Aldrich, I9278), 0.5mM 3-isobutyl-1-methylxanthine (IBMX, Sigma-Aldrich, I5879), 5μM

dexamethasone (Sigma-Aldrich, D4902), 0.125mM indomethacin (Sigma-Aldrich, I8280), 50nM T3 (Sigma-Aldrich, T2877), and 1μM rosiglitazone (Sigma-Aldrich, R2408) for two days and subsequently cultured in maintenance medium supplemented with 5μg/ml insulin, 50nM T3 and 1μM rosiglitazone. Primary preadipocytes were induced to differentiate with an adipogenic cocktail (6μg/ml insulin, 0.5mM IBMX, 1μM dexamethasone, 50nM T3, and 1μM rosiglitazone) in DMEM medium containing 10% FBS, 1% pen/strep for two days and subsequently maintained in maintenance medium containing 50nM T3, 1μM rosiglitazone and 6μg/ml insulin. Immortalized beige preadipocytes were induced to differentiate to beige adipocytes in differentiation medium supplemented with 5μg/ml insulin, 0.5mM IBMX, 1μM dexamethasone, and 1μM rosiglitazone for two days and subsequently cultured in maintenance medium supplemented with 1 μM rosiglitazone and 5 μg/ml insulin. Immortalized brown preadipocytes were induced to differentiate to brown adipocytes in differentiation medium supplemented with 1μg/ml insulin, 0.5mM IBMX, 1μM dexamethasone, 0.125mM indomethacin, 1nM T3 and 1μM rosiglitazone for two days and subsequently cultured in maintenance medium supplemented with 1 nM T3 and 1 μg/ml insulin. The maintenance medium was changed every two days and mature adipocytes were collected on seventh day.

To investigate cellular thermogenesis, differentiated adipocytes on plates were maintained in a water bath for homogenized temperature changing inside incubator set at 41°C (HT) or 37°C (Con) for 0.5, 1 or 2 h. Both HT and Con cells were then placed back to 37°C. After 12 h, differentiated adipocytes were collected for gene expression analysis, cellular viability analysis (Cell Counting Kit-8, Beyotime, C0041) or treated with ERthermAC dye (250 nM, Emdmillipore, SCT057) for 30 min and subjected to FACS analysis (BD LSR Fortessainstrument).

METHOD DETAILS

Metabolic analysis in mice

Mice (8 weeks) were fed with chow diet or HFD (60%, ResearchDiet, D12492) for indicated time. For assessing metabolic parameters, body weight, and body compositions were measured once a week using AccuFat MRI system (AccuFat-1050, MAG-MED). Oxygen consumption, food intake and locomotor activity were measured in Comprehensive Lab Animal Monitoring System (CLAMS, Columbus Instruments).

For cold exposure, mice were housed at 4°C and core temperature were measured at indicated time. For glucose tolerance test, mice were fasted overnight and injected intraperitoneally with a glucose solution in saline (1.25 g/kg body weight). For insulin tolerance test, mice received an intraperitoneal injection of insulin at 1.25 or 1.5U/kg body weights. Blood glucose levels were measured at 0, 15, 30, 60, 90 and 120 m after injection with an automated reader (Bayer).

To measure liver triglyceride contents, liver tissues were homogenized in 5% NP40 in PBS. Tissue lysates were centrifuged and the supernatant liquid were obtained and triglyceride levels were determined by Triglycerides kit (BioVision, K622) and normalized to liver protein content using BCA protein assay kit (Beyotime, P0012).

Serum parameters were measured via colorimetric assays with commercially available kits including serum triglyceride (TG, BioVision, K622), total cholesterol (TC, Sigma-Aldrich, MAK043), high-density lipoprotein cholesterol (HDL, Sigma-Aldrich, MAK045), low-density lipoprotein cholesterol (LDL, Sigma-Aldrich, MAK045), Alanine aminotransferase (ALT, Sigma-Aldrich, MAK052), Aspartate aminotransferase (AST, Sigma-Aldrich, MAK055), Creatine kinase (Sigma-Aldrich, MAK116), Uric acid (Sigma-Aldrich, MAK077), Creatinine (Sigma-Aldrich, MAK080), Urea nitrogen (Sigma-Aldrich, MAK006), Albumin (Sigma-Aldrich, 09753), Total protein (Sigma-Aldrich, 71285-M), Alkaline phosphatase (Abcam, ab83369), Amylase (Sigma-Aldrich, MAK009) and Lactate dehydrogenase (Sigma-Aldrich, MAK066). Serum and iWAT norepinephrine (NE) levels were determined by ELISA kit (CUSABIO, CSB-E07870m). Serum Cortisol levels were measured using a commercial ELISA kit (CUSABIO, CSB-E05113m).

Thermal image analysis

Thermal images analysis was performed as previously reported (Symonds et al., 2012). Briefly, the thermal images were imported into FLIR software to define the area of interest, which is the supraclavicular fat area in human and the inguinal fat area in mouse. Radiometric temperature data from the defined area were exported. The thermal images were identified with the hottest 10% points among supraclavicular area temperature in human or inguinal fat area temperature in mouse and mean values were calculated with mean value of those unified points.

Measurement of NE turnover

NE turnover was measured on the basis of the decline in tissue NE content after the inhibition of catecholamine biosynthesis with α-methyl-p-tyrosine (α-MT) as described previously (Shiuchi et al., 2009). After 10 min LHT or Sham on iWAT, mice were either i.p. injected with α-MT (200 mg/kg, Sigma-Aldrich, M3281). Prior or 4 h after α-MT injection, the animals were sacrificed and iWAT were removed, weighed, and homogenized in 0.2 M perchloric acid containing 0.1 mM EDTA. The homogenates were centrifuged at 4°C and the NE content of the supernatants was assayed by ELISA (CUSABIO, CSB-E07870m) and normalized to iWAT weights.

Blood flow measurements in mice

Mice were injected with PDA/PEG hydrogel (PDA) bilaterally in iWAT prior to blood flow measurement. For the analysis of iWAT and BAT blood flow after LHT on iWAT, mice were anesthetized with 75 mg/kg pentobarbital sodium with i.p. injection and the fur over the interscapular or inguinal regions were carefully removed. Skin areas covering beige fat were illuminated unilaterally on one side of

iWAT with NIR laser for 10 m (LHT) while the other side of iWAT remained unilluminated (Sham). Afterwards, the animals were placed in the supine (for iWAT studies) or prone (for BAT studies) position for blood flow measurements by HR-LDI (Moor Instruments) at the speed of 4 ms/pixel over the area of iWAT or BAT as previously reported (Abreu-Vieira et al., 2015). Acquired images were analyzed with MoorLDI Image Processing software (research version 5.3).

Fecal bomb calorimetry

Mice were housed individually with less padding and feces were collected over a 24-hour period. Then feces were dehydrated for 48 h and heat of combustion was determined using an automatic oxygen bomb calorimeter (Parr 6400). Benzoic acid standards were used to determine the calorimeter energy equivalent factor. The sample calory was normalized to dry feces weight.

Lentivirus-mediated gene transfer

HSF1 wild-type (CC), p.Pro365Thr (AA), psPAX2, and pMD2.G were used for lentiviral package. High-titer lentivirus were packaged in 293T cells using lipofectamine2000 transfection agent. Viral supernatants were collected and concentrated by centrifugation and used for adipocytes infection and mouse adipose tissue delivery.

Plasmid construction

Active form of HSF1 plasmid was constructed by deleting amino acids 186-202 of HSF1 (Jung et al., 2008) and cloned in pcDNA3.1 vector. Point mutation of HSF1 with substitution of Pro to Thr at 365AA (Pro365Thr) were generated by site-directed mutagenesis (Vazyme, C215). The luciferase reporter A2B1-Luc (-2007 to +261) and the putative HSE deletion reporter A2B1-dHSE-Luc (-207 to -195) was cloned into PGL4.17 basic vector. The Pgc1α /Ucp1 3′UTR or Pgc1α/Ucp1 3′UTR with deletion of the putative A2B1 binding motif were cloned into pMIR-REPORTTM. Primer pairs for plasmid construction were listed in Table S4.

RNA Extraction, quantitative PCR, PCR array, and RNA-seq

Total RNA was extracted from cultured cells or tissues with RNAiso Plus (TaKaRa, 9108), and 1 μg total RNA was reverse transcribed to cDNA using the PrimeScript™ RT Master Mix (TaKaRa, RR036A) according to the manufacturers' instructions. Quantitative Real-time PCR was performed using the Hieff® qPCR SYBR Green Master Mix (Low Rox Plus) (Yeasen, 11202ES03) on the Roche Light-Cycler480 (Roche). Experiments were repeated three times and gene expression levels were calculated using the delta Ct method, after normalization to 36B4 expression. Sequences of primers used for real-time PCR are listed in Table S4. PCR array regarding adipocyte functionality was purchased from Qiagen (PAMM-049Z).

For RNA-seq, RNA quality was examined with a Nanodrop spectrophotometer (Thermo, MA, USA) and agarose gel electrophoresis. High quality RNA was used to construct library and Illumina NovaSeq6000 was used to perform RNA-seq (Genergy Biotechnology, Shanghai, China). Briefly, RNA libraries were constructed by TruSeq® RNA LT Sample Prep Kit v2 (illumina, USA) following the manufacturer's protocol and quantified by Qubit (invitrogen, USA) for cluster generation. Processed RNA-seq data were filtered by removing genes with low read counts. Read counts were normalized using TMM normalization and CPM (counts per million) were calculated to create a matrix of normalized expression values. p-value <0.05 and |FC| >= 2 were used to determine differential genes. GO enrichment analysis was performed by clusterProfiler (v3.12.0) (Yu et al., 2012). p-value <0.05 was considered as significantly enrichment.

Immunoblotting

Cells and tissues were lysed in RIPA lysis buffer (Thermo Fisher, 89900) containing PMSF (Thermo Fisher, 36978) and protease inhibitors (Thermo Fisher, A32963). Total protein lysates were boiled with loading sample buffer containing 10% SDS-PAGE. Subsequently, separated proteins were transferred onto PVDF membranes. PVDF membrane blots were blocked in 10% skimmed milk for 1 h at room temperature, washed in Tris-buffered saline with Tween 20 (TBS-T) and incubated overnight at 4°C with rabbit anti-UCP1 (Abcam, ab10983), anti-HSF1 (CST, 4356S), anti-HNRNPA2B1 (Abcam, ab31645), mouse anti-PGC1α (Santa Cruz, sc-517380) or anti-β-ACTIN (Sigma-Aldrich, A3854). Anti-rabbit IgG (LI-COR, 926-68071) was used as the second antibody for UCP1, HSF1 and HNRNPA2B1. Anti-mouse IgG (LI-COR, 926-32210) was used as the second antibody for PGC1α and β-ACTIN.

Immunofluorescence

Immortalized beige adipocytes were cultured on coverslip in 48-well plates and fully differentiated, fixed, permeabilized, and incubated with primary antibodies against HSF1 and UCP1 (mouse anti-HSF1, Santa cruz, sc-17757; rabbit anti-UCP1, Abcam, ab10983) overnight at 4°C. Cells were washed and incubated with goat anti-mouse Alexa Fluor 594 (Thermo Fisher, A11032) and goat anti-rabbit Alexa Fluor 488 (Thermo Fisher, A11034) for 1 h at room temperature. DAPI was used to visualize the nuclei. Images were taken using a Leica confocal microscope and processed using ImageJ.

Oil Red O staining and quantitative analysis

Cells were fixed with 10% paraformaldehyde and washed twice with PBS and rinsed with 60% isopropanol, then stained with a filtered Oil Red O working solution (Sigma-Aldrich, O0625) for 20 min at room temperature. After the cells were photographed, the Oil Red O was eluted with 60% isopropanol for 30 min at room temperature. The optical density (OD) value of each well at 520 nm was measured with colorimetric assay on BMG Labtech SPECTROstar Nano.

ChIP and ChIP-seq assays

For ChIP-seq, ChIP assays were first performed using a SimpleChIP® Plus Enzymatic Chromatin IP Kit (CST, 9003) according to manufacturer's instructions. In brief, differentiated C3H10T1/2-derived beige adipocytes or immortalized beige adipocytes were cross-linked by 1% formaldehyde for 10 min and stopped by glycine. The extracted chromatin was digested and fragmented into 200 to 1000 bp, which was then immunoprecipitated by ChIP grade antibodies anti-HSF1 (CST, 4356S) or normal IgG (CST, 2729) using Magnetic Beads. After that, samples were uncrosslinked to obtain pure DNA fragment and ChIP-seq analysis was performed by Genergy Biotechnology (Shanghai, China) using illumina Hiseq3000. Quality control was processed by FastQC software (Andrews, 2010). Then the filtered sequencing reads were mapped to the mouse reference (mm10) using Bowtie2 (v.2.2.5) (Langmead and Salzberg, 2012). For peak calling, MACS2 (v2.1.1) (Zhang et al., 2008) was used to scan peaks in genomic-wide level according to each IP (treatment) and Input (control) pair. Finally, visualization is performed by Integrative Genomic Viewer genome (IGV) browser (v.2.8.0) (Robinson et al., 2011) using BigWig tracks. ChIP analysis was performed using same kit and protocols without sequencing. ChIP primers were listed in Table S4.

RNA immunoprecipitation assay

RNA immunoprecipitation (RIP) assay was performed with Magna RIP RNA-Binding Protein Immunoprecipitation Kit (Millipore, 17-700) according to manufacturer's instructions. Briefly, fully differentiated immortalized beige or brown adipocytes were washed with ice-cold PBS and resuspended in RIPA lysis buffer (containing RNase inhibitor, Millipore, CS203219). The extract was precleared with Sepharose beads and subjected to immunoprecipitation with HNRNPA2B1 antibody (Abcam, ab31645). After extensive washing with RIP washing buffer (containing RNase inhibitor, Millipore, CS203219), co-precipitated RNAs were purified. The RNA samples precipitated were extracted, reversed transcribed, and subjected to RT-qPCR analysis.

Luciferase reporter assay

HEK293T cells (ATCC) were transfected with indicated plasmids and luciferase reporter together with Renilla luciferase control reporter by EZ-Trans transfection reagent. Cells were collected with passive lysis buffer (Promega, E1960) and luciferase assays were performed using a dual luciferase reporter assay kit (Promega, E1960).

Histological analysis

Dissected adipose and liver tissues were fixed in 10% neutral buffered formalin (Sigma-Aldrich, HT501128-4L) and embedded in paraffin. 5μm tissue sections were stained with Hematoxylin and eosin (Beyotime, C0105S) according to manufacturer's instructions. The images were acquired by optical microscope (Nikon) using a 20x objective. Adipocyte sizes were quantified by ImageJ.

Preparation of PDA-PEG hydrogel

The PDA-PEG hydrogel (PDA) was prepared as previously reported (Wang et al., 2017). Briefly, PDA nanoparticles were prepared via a spontaneous oxidative polymerization of dopamine under alkaline condition. Subsequently, 0.5 mL PDA nanoparticles (50 mg/mL) and 0.5 mL 4-arm-PEG-SH (100 mg/mL) both in aqueous solution were mixed and blended on a Vortex mixer for 5 m. The mixture was kept at 4°C without disturbance or immediately used for injection.

siRNA transfection

siRNA was designed and synthesized by GenePharma (Shanghai, China). siRNA was transfected into differentiated adipocytes using Lipofectamine2000 Transfection Reagent (Thermo Fisher, 11668030) according to the manufacturer's protocol. The gene expression analysis was determined by RT-qPCR after 48 h.

RNA stability assay

Differentiated immortalized beige adipocytes were transfected with siNC or siRNA against *Hnrnpa2b1* or adenovirus mediated *Hnrnpa2b1* overexpression (Hanbio biotechnology, Shanghai, China) for two days. Cells were treated with 5μg/ml actinomycin D (Sigma-Aldrich, SBR00013) and harvested at indicated time points. The total RNA was isolated and analyzed by RT-qPCR. The degradation rate of mRNA K_d was estimated by: $\ln(C_t/C_0) = -K_d t$, where t is the time as actinomycin D treatment for transcription inhibition. C is the mRNA concentration. The mRNA half-life $t_{1/2}$ is calculated by: $t_{1/2} = \ln 2/K_d$.

QUANTIFICATION AND STATISTICAL ANALYSIS

Statistics were computed with GraphPad Prism 7 software. The statistical details of experiment are indicated in the figure legend. The normalcy of data was examined by Shapiro-Wilk normality test. Statistical comparisons between two groups were made by unpaired Student's t-test. Paired t-test was used for assessing the difference of temperature change between the same subject in Sham and LHT group. Two-way ANOVA with Bonferroni's multiple comparisons was used for comparisons of multiple factors and ANCOVA was used to analyze oxygen consumption data by SPSS software (Butler and Kozak, 2010; Mina et al., 2018; Tschöp et al., 2011). Results are shown as mean ± SEM. $p<0.05$ was considered as statistically significant, $^{*}p<0.05$, $^{**}p<0.01$.

Supplemental figures

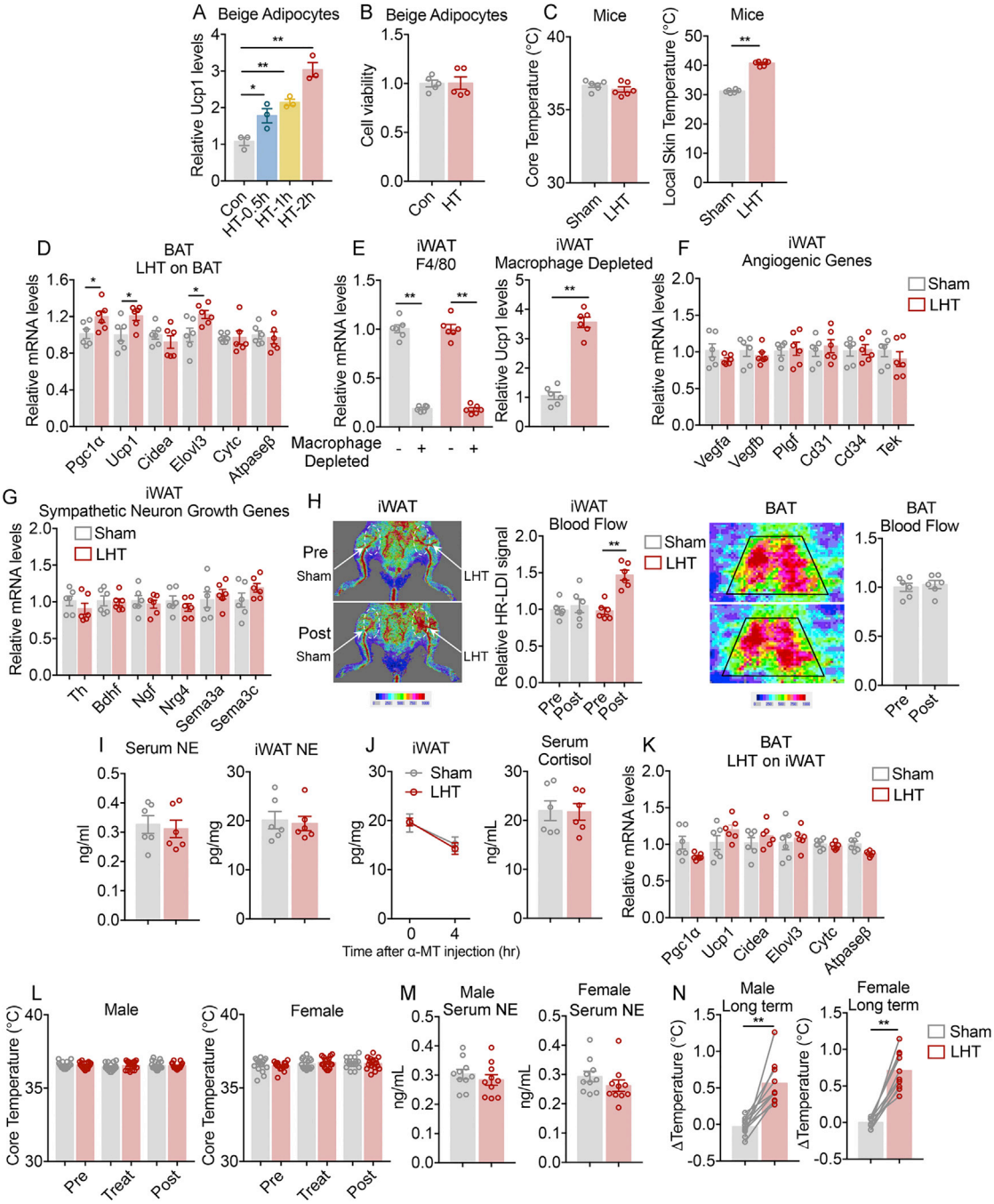

Figure S1. Thermogenesis induced by hyperthermia *in vivo* is independent of central sympathetic and immune systems, related to Figure 1

(A) *Ucp1* mRNA levels in C3H10T1/2-derived beige adipocytes treated with 37°C (Con) or 41°C hyperthermia therapy (HT) for 0.5, 1, or 2 h (n = 3) and rest for 12 h.

(B) The cellular viability of C3H10T1/2-derived beige adipocytes treated with or without HT for 2 h and rest for 12 h were evaluated by CCK8 assays (n = 5).

(C) The body core temperature change (left) and local skin temperature change (right) of mice unilaterally treated with Sham or LHT for 10 min (n = 6).

(D) mRNA levels of thermogenic and mitochondrial genes in BAT of mice with 10-min Sham or LHT on BAT and rest for 24 h (n = 6).

(E) *F4/80* (left) and *Ucp1* (right) mRNA levels in mice with Sham or LHT for 10 min and rest for 24 h with or without iWAT macrophage depletion via 110 mg/kg clodronate-loaded liposome injection in iWAT for three times (n = 6).

(legend continued on next page)

(F and G) mRNA levels of angiogenic (F) and sympathetic neuron growth (G) gene programs in iWAT of mice with Sham or LHT for 10 min and rest for 24 h.
(H) Visualization of iWAT and BAT blood flow by high-resolution laser-Doppler imaging (HR-LDI) pre- or post-unilateral iWAT Sham or LHT for 10 min and quantification (n = 6).
(I and J) Serum and iWAT norepinephrine (NE) levels, NE turnover in iWAT and serum cortisol levels of mice acutely treated with Sham or LHT for 10 min (n = 6).
(K) mRNA levels of thermogenic and mitochondrial genes in BAT of mice with 10-min Sham or LHT on iWAT and rest for 24 h (n = 6).
(L) The core temperature of human pre-, mid-, and post-Sham/LHT treatment (male, n = 17; female, n = 16).
(M) Serum NE of subjects post-Sham or LHT (male, n = 10; female, n = 10).
(N) Quantification of temperature changes of human supraclavicular area (ΔTemperature, post-pre) under Sham or 5 weeks LHT (male, n = 10; female, n = 10).
Statistical significance was assessed by unpaired Student's t test (A–I, J right, and K–M), two-way ANOVA (J left), or paired Student's t test (N). Data are presented as mean ± SEM and *$p < 0.05$, **$p < 0.01$.

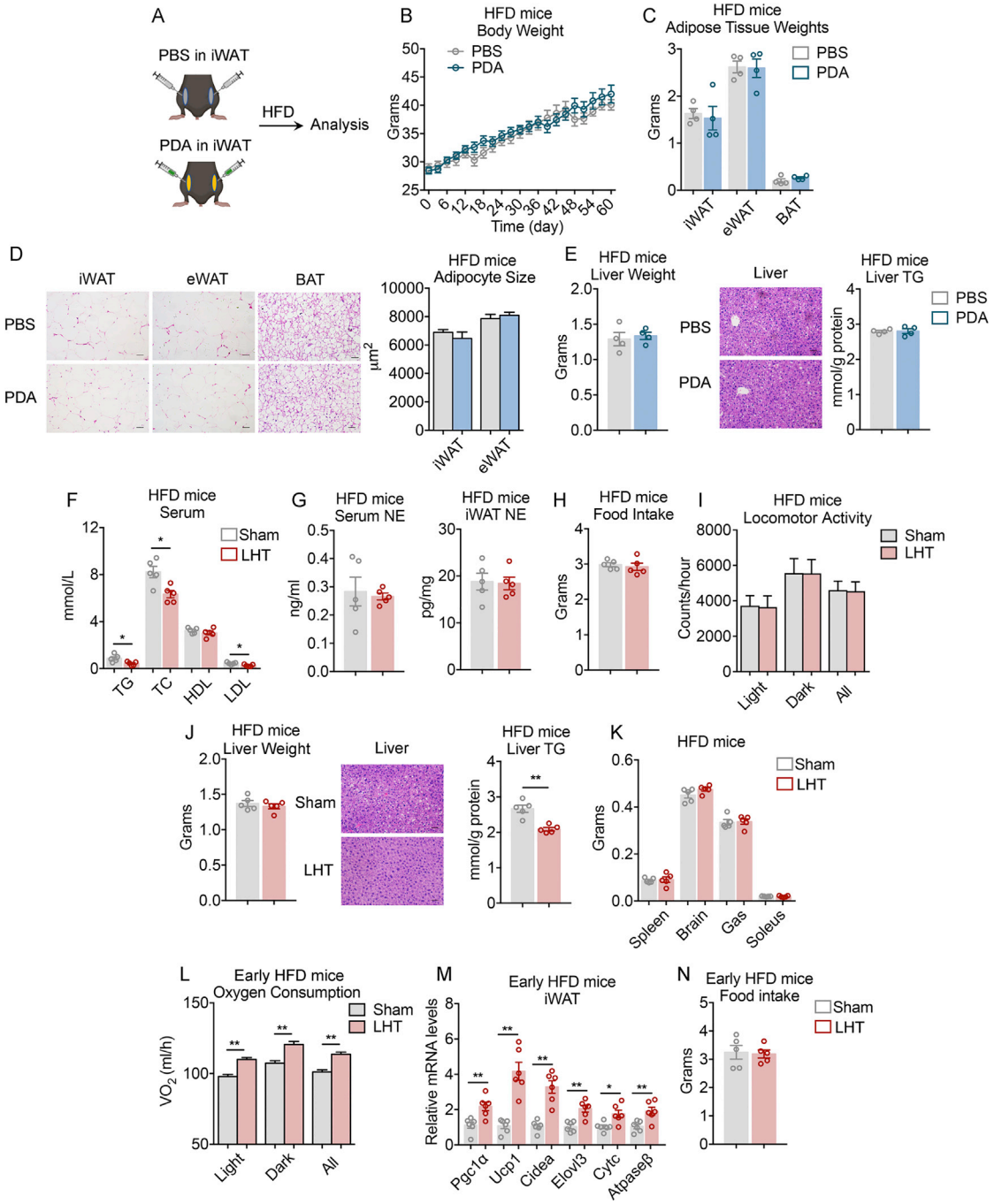

Figure S2. Chronic injection of PDA shows no obvious adverse effect on mice, and LHT ameliorates serum parameters and hepatic steatosis in HFD mice, related to Figure 2

(A) Schematic figure of mice injected with PBS or PDA in bilateral iWATs on HFD to examine the toxic effects of PDA.

(B–E) Mice injected with PBS or PDA in inguinal fat on HFD (n = 4), including (B) body weight; (C) adipose tissue weights; (D) representative H&E staining of adipose tissues; and (E) liver weight, representative H&E staining of liver and hepatic TG levels.

(F–K) Analysis of metabolic parameters of mice treated following the same treatment as in Figure 2A for over 10 weeks (n = 5), including (F) serum total cholesterol (TG), total cholesterol (TC), high-density lipoprotein (HDL), and low-density lipoprotein (LDL) levels; (G) NE levels in serum (left) and iWAT (right); (H) food intake; (I) locomotor activity; (J) liver weight, representative H&E staining of liver and hepatic TG levels; and (K) organ weights.

(L–N) Analysis of metabolic parameters of mice treated following the same treatment as in Figure 2A for 1 week (early HFD) (n = 5), including (L) oxygen consumption; (M) mRNA levels of thermogenic and mitochondrial genes; and (N) food intake.

Statistical significance was assessed by two-way ANOVA followed with Bonferroni's multiple comparison test (B) or unpaired Student's t test (C–K, M, and N) or ANCOVA with body weight as covariant (L). Scale bars, 50 μm. Data are presented as mean ± SEM and *p < 0.05 and **p < 0.01.

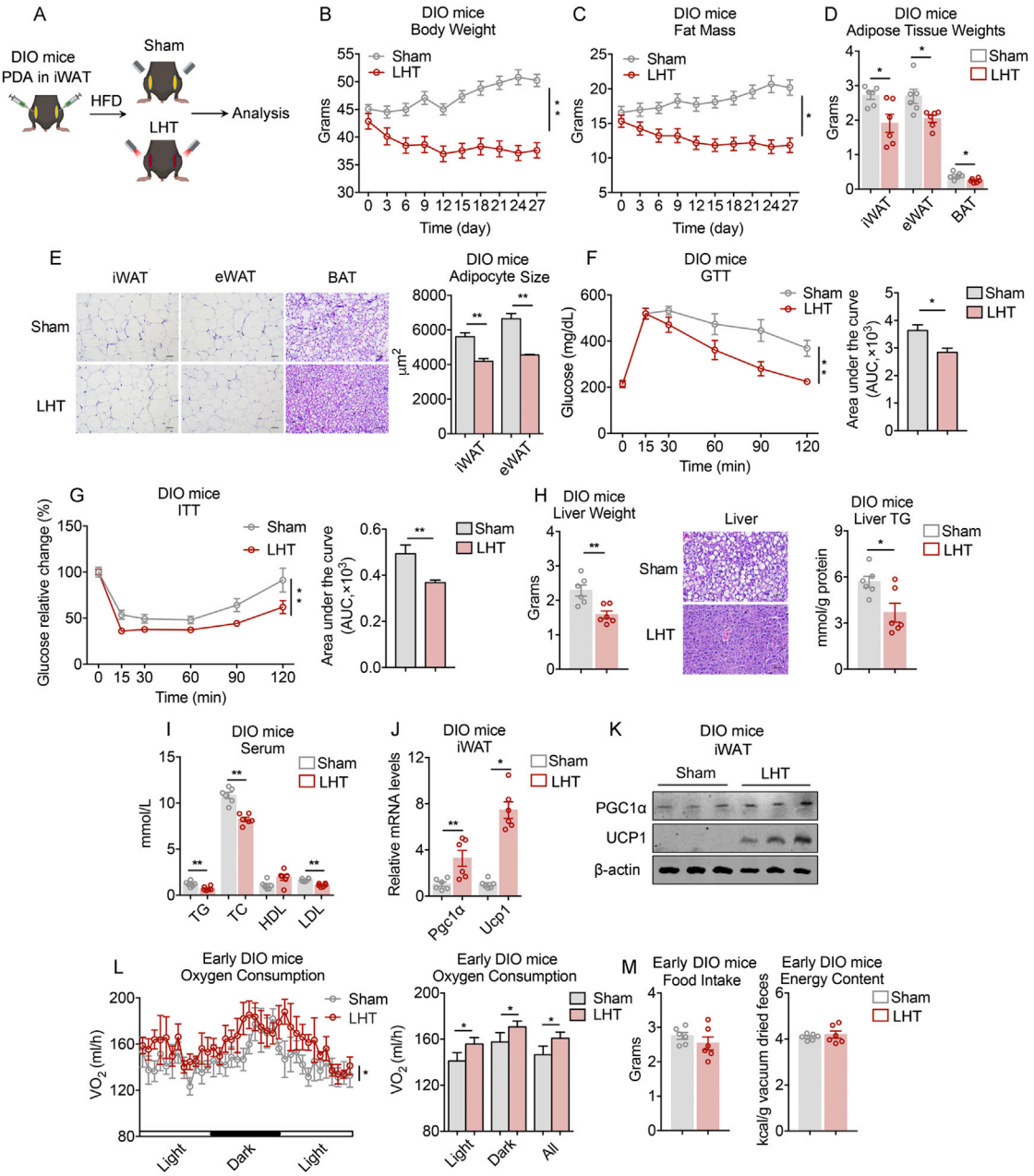

Figure S3. LHT improves the metabolic dysfunctions in diet-induced obesity (DIO) mice, related to Figure 2

(A) Schematic figure of DIO mice: HFD feeding to over 40 g with iWAT bilateral injection with PDA and treated chronically without NIR illumination (Sham) or with 10 min NIR laser (LHT) on each side of iWAT once every 3 days.

(B–I) Analysis of metabolic performances of DIO mice following the treatment as in (A) for over 4 weeks (n = 6), including (B) body weight; (C) fat mass; (D) adipose tissue weights; (E) representative H&E staining of adipose tissues; (F) GTT; (G) ITT; (H) liver weight, representative H&E staining of liver tissues and hepatic TG; and (I) serum parameters TG, TC, HDL, and LDL levels.

(J and K) Analysis of mRNA and protein levels of Pgc1α and Ucp1 in iWAT of DIO mice following the treatment as in (A) for over 4 weeks (n = 6).

(L and M) Analysis of metabolic parameters of DIO mice following the treatment as in (A) for 1 week (early DIO) (n = 6), including (L) oxygen consumption and (M) food intake and fecal energy content.

Statistical significance was assessed by two-way ANOVA followed with Bonferroni's multiple comparisons test (B, C, F, and G) or unpaired Student's t test (D, E, H, I, J, and M) or ANCOVA with body weight as covariant (L). Scale bars, 50 μm. Data are presented as mean ± SEM and *p < 0.05 and **p < 0.01.

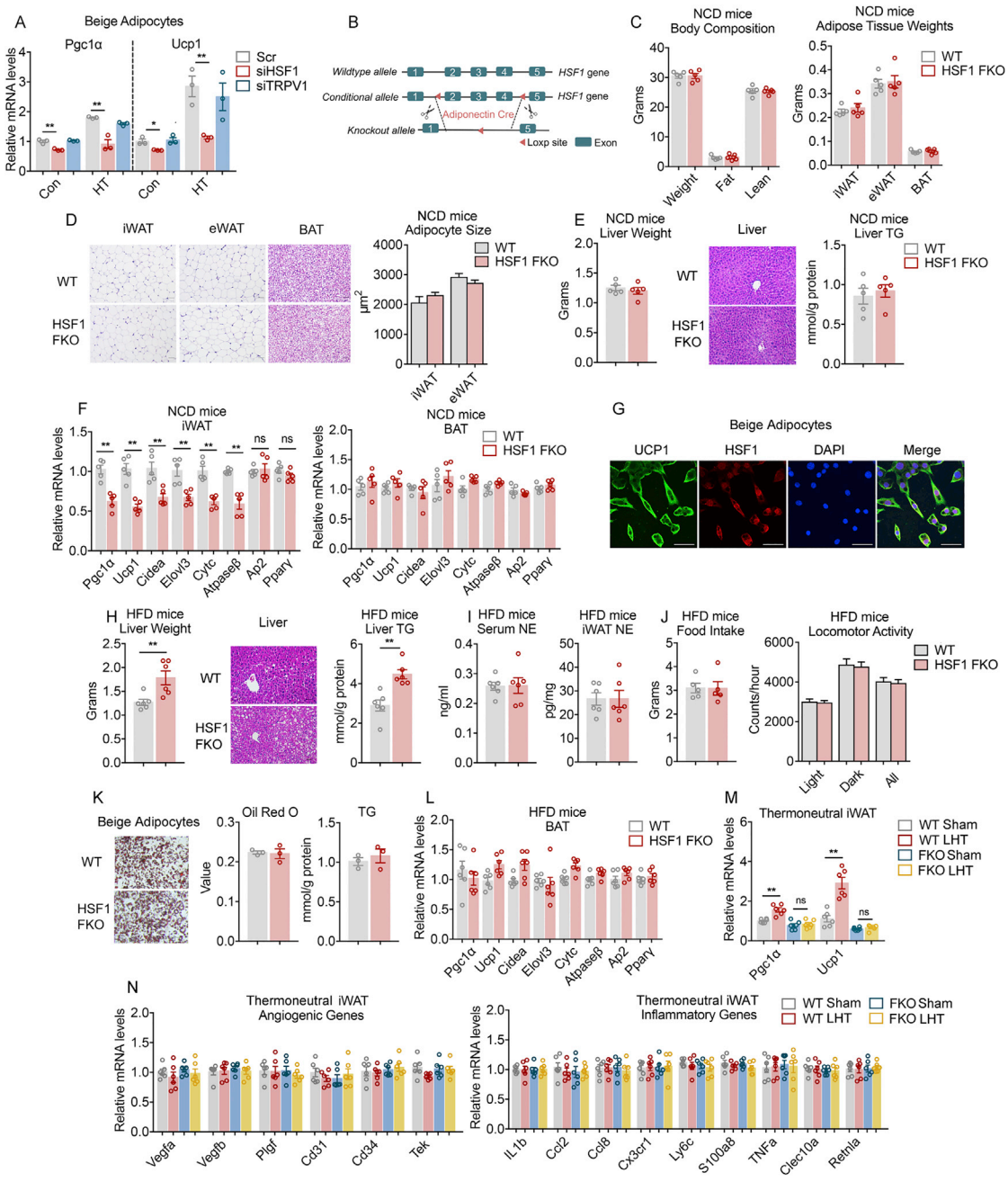

Figure S4. Metabolic parameters of HSF1 FKO mice under normal chow diet (NCD), related to Figure 3

(A) mRNA levels of *Pgc1α* and *Ucp1* in scramble (Scr) and Hsf1 knockdown (siHSF1) or Trpv1 knockdown (siTRPV1) immortalized beige adipocytes under control or HT condition (n = 3).

(B) Construction strategy of Adiponectin-Cre Hsf1$^{loxp/loxp}$ mice for HSF1-specific knockout in fat (HSF1 FKO).

(C–F) Analysis of metabolic parameters of WT and HSF1 FKO mice on NCD at 8 weeks of age (n = 5), including (C) body weight, body compositions (left), and adipose tissue weights (right) and (D) representative H&E staining of adipose tissues. (E) Liver weight, H&E staining of liver and hepatic TG levels. (F) mRNA levels of thermogenic, mitochondrial, and adipogenic gene programs in iWAT and BAT.

(G) Immunofluorescence staining of HSF1 and UCP1 in differentiated primary beige adipocytes under basal condition.

(H) Liver weight, H&E staining, and hepatic TG levels of WT and HSF1 FKO mice on HFD (n = 6).

(I) Serum (left) and iWAT (right) NE levels of WT and HSF1 FKO mice on HFD (n = 6).

(J) Food intake and locomotor activity measured by CLAMS of WT and HSF1 FKO mice on HFD (n = 5).

(K) Oil red O staining and TG levels of differentiated primary beige adipocytes from WT and HSF1 FKO mice (n = 3).

(L) mRNA levels of thermogenic, mitochondrial, and adipogenic gene programs in BAT from WT and HSF1 FKO mice on HFD (n = 6).

(legend continued on next page)

(M and N) mRNA levels of *Pgc1α* and *Ucp1*(M), angiogenic and inflammatory genes (N) in iWAT from WT and HSF1 FKO mice kept under thermoneutral conditions of 30°C (n = 6).

Statistical significance was assessed by unpaired Student's t test (A, C–F, and H–N). Scale bars, 50 μm (D, E, H, and K) and 30 μm (G). Data are presented as mean ± SEM and *$p < 0.05$ and **$p < 0.01$.

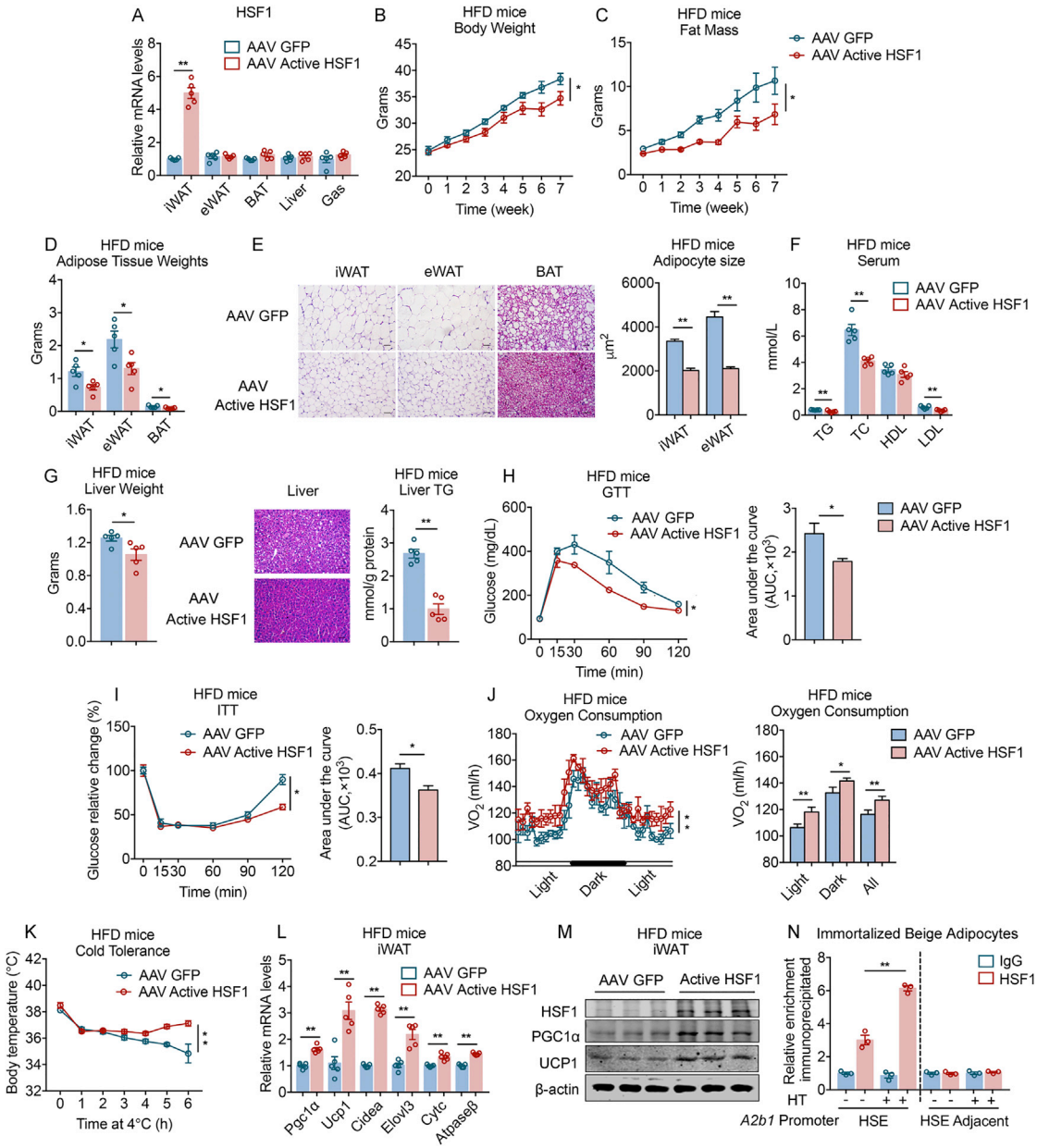

Figure S5. AAV-mediated active form of HSF1 overexpression in iWAT promotes browning of white fat and energy metabolism, related to Figure 3

(A) Hsf1 expression in metabolic organs after AAV mediated GFP (AAV GFP) or active form of HSF1 (AAV Active HSF1) delivery in iWAT (n = 5).

(B–M) Analysis of metabolic parameters of C57BL/6J mice with inguinal fat pad injection of AAV-mediated GFP or active form of HSF1 overexpression on HFD (n = 5), including (B) body weight; (C) fat mass; (D) adipose tissue weights; (E) representative H&E staining of adipose tissues; (F) serum parameters of TG, TC, HDL, and LDL levels; (G) liver weight, representative H&E staining of liver and hepatic TG levels; (H) GTT; (I) ITT; (J) oxygen consumption; (K) cold tolerance test; (L) mRNA levels of thermogenic and mitochondrial genes; and (M) immunoblotting for HSF1, PGC1α, and UCP1 proteins in iWAT.

(N) ChIP assay assessing HSF1 binding on the putative HSE region of the *A2b1* promoter in immortalized beige adipocytes (n = 3).

Statistical significance was assessed by unpaired Student's t test (A, D–G, L, and N), ANCOVA with body weight as covariant (J) or two-way ANOVA followed with Bonferroni's multiple comparison test (B, C, H, I, and K). Scale bars, 50 μm. Data are presented as mean ± SEM and *p < 0.05 and **p < 0.01.

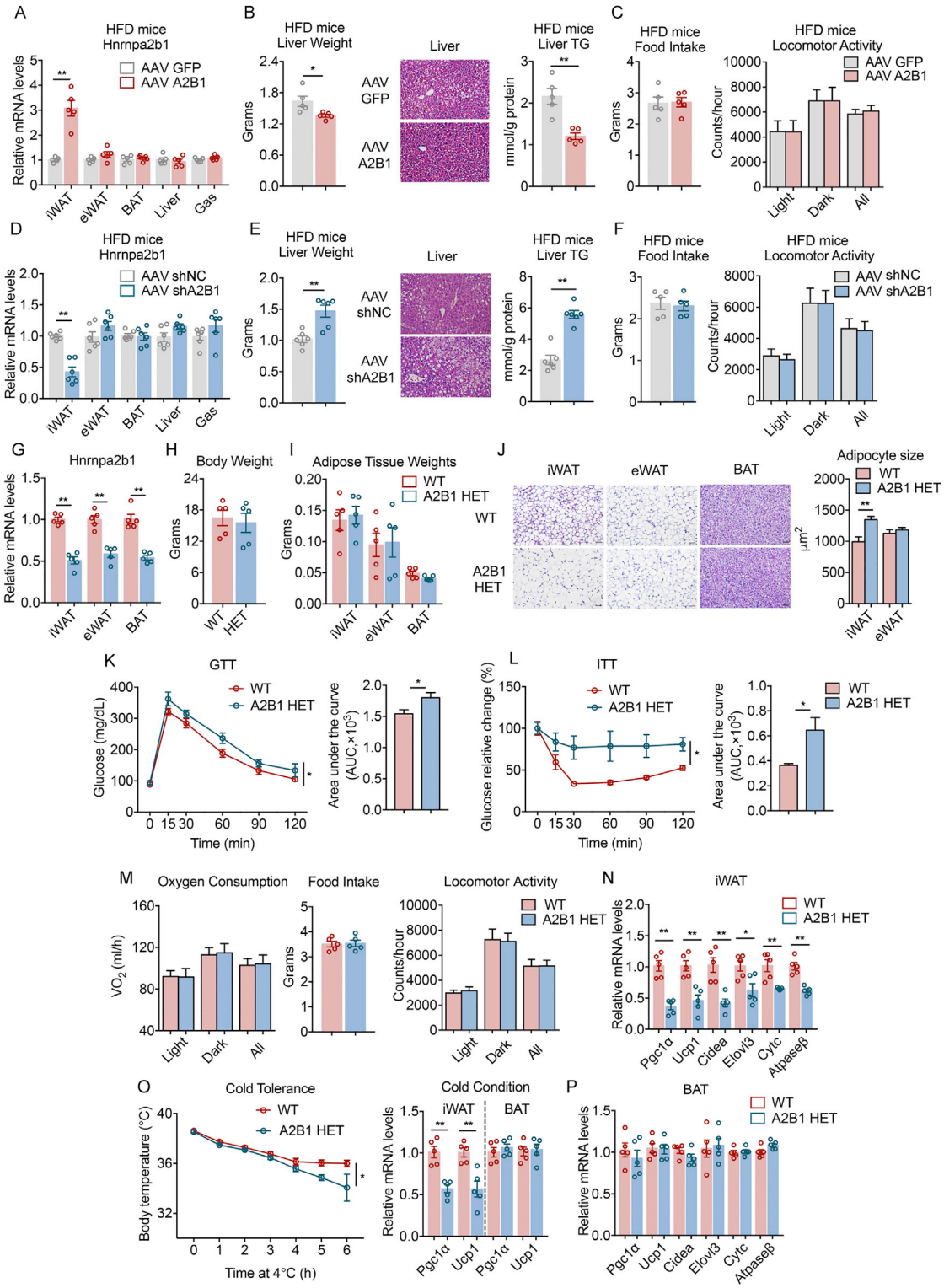

Figure S6. HNRNPA2B1 promotes browning of white fat and energy metabolism, related to Figure 5

(A–C) Analysis of metabolic parameters of C57BL/6J mice with iWAT injection of AAV-mediated GFP (AAV GFP) or HNRNPA2B1 (AAV A2B1) on HFD (n = 5), including (A) Hnrnpa2b1 expression levels in metabolic organs; (B) liver weight, representative H&E staining of liver and hepatic TG levels; and (C) food intake and locomotor activity measured in CLAMS.

(legend continued on next page)

(D–F) Analysis of metabolic parameters of C57BL/6J mice with iWAT injection of AAV-mediated scrambled control (AAV shNC) or HNRNPA2B1 knockdown (AAV shA2B1) on HFD (n = 6), including (D) *Hnrnpa2b1* expression levels in metabolic organs (n = 6); (E) liver weight, representative H&E staining of liver and hepatic TG levels (n = 6); and (F) food intake and locomotor activity measured in CLAMS (n = 5).

(G) *Hnrnpa2b1* mRNA levels in adipose tissues of wild-type and Hnrnpa2b1 heterozygous (A2B1 HET) mice (n = 5).

(H–P) Analysis of metabolic parameters of wild-type and Hnrnpa2b1 heterozygous mice on NCD at 4 weeks old (n = 5), including (H) body weight; (I) adipose tissue weights; (J) representative H&E staining of adipose tissue; (K) GTT; (L) ITT; (M) oxygen consumption, food intake, and locomotor activity; (N) mRNA levels of thermogenic and mitochondrial genes in iWAT; (O) cold tolerance test as well as *Pgc1α* and *Ucp1* mRNA expression in BAT and iWAT upon cold exposure; and (P) mRNA levels of thermogenic and mitochondrial genes in BAT.

Statistical significance was assessed by unpaired Student's t test (A–J, N, and P) or two-way ANOVA followed with Bonferroni's multiple comparisons test (K, L, and O) or ANCOVA with body weight as covariant (M). Scale bars, 50 μm. Data are presented as mean ± SEM and *$p < 0.05$ and **$p < 0.01$.

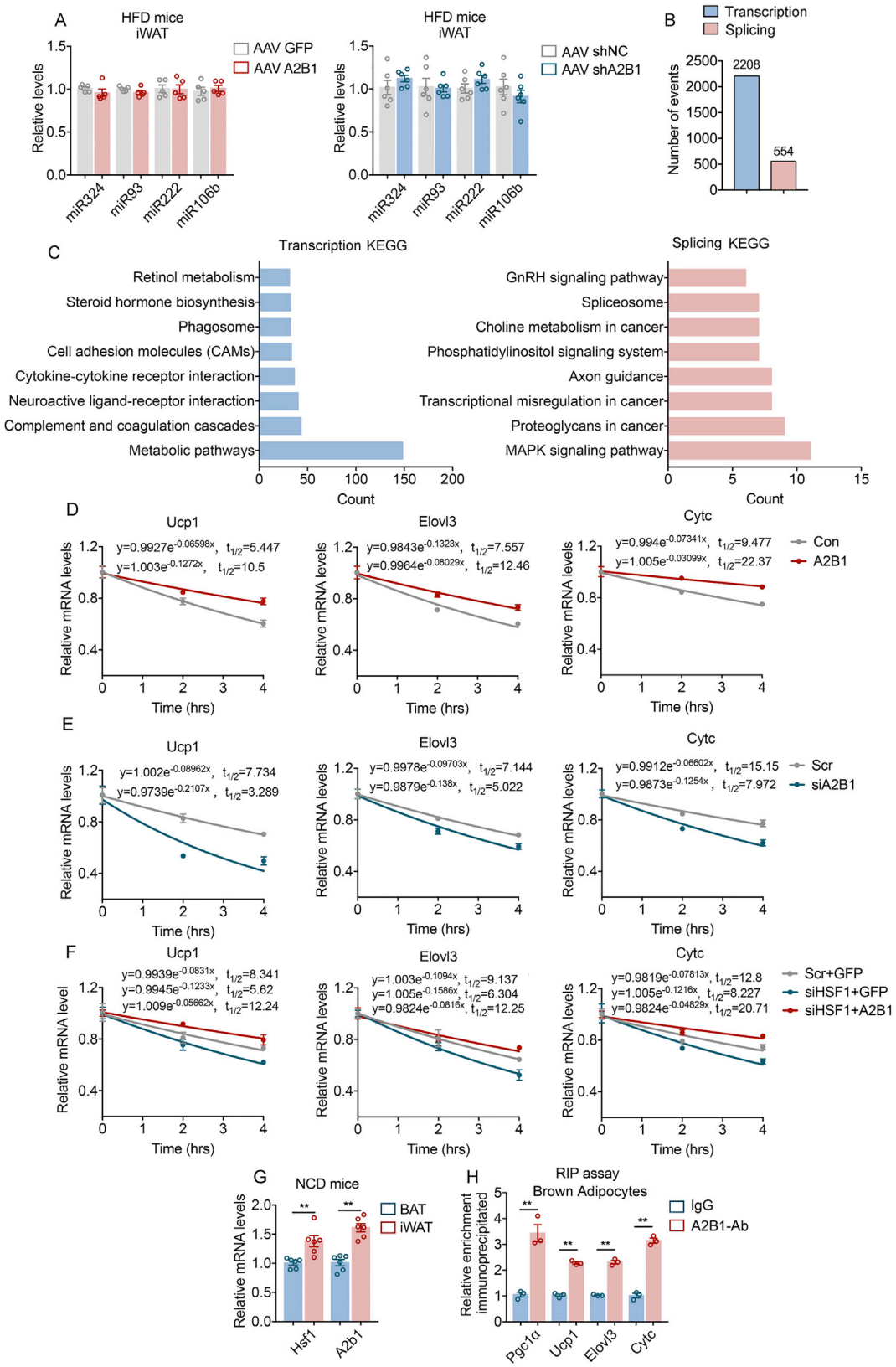

(legend on next page)

Figure S7. HNRNPA2B1 regulates gene transcription in beige adipocytes rather than miRNA processing or alternative splicing, related to Figure 6

(A) Reported HNRNPA2B1 (A2B1) target miRNA levels after A2B1 overexpression (n = 5) or knockdown (n = 6) compared with their controls.

(B) RNA-seq data in transcriptional gene expression changes (fold change > 2 and p value < 0.05) and alternative splicing events (PSI > 0.1, p value < 0.05) in iWAT overexpressing GFP or A2B1.

(C) KEGG pathway enrichment analysis of top changed transcriptional or splicing gene categories in iWAT overexpressing A2B1 compared with GFP.

(D) mRNA levels of *Ucp1*, *Elovl3*, and *Cytc* in control (Con) and A2B1 overexpression immortalized beige adipocytes upon transcriptional inhibition with actinomycin D at indicated time (n = 4).

(E) mRNA levels of *Ucp1*, *Elovl3*, and *Cytc* in scramble (Scr) and A2B1 knockdown (siA2B1) immortalized beige adipocytes upon transcriptional inhibition with actinomycin D at indicated time (n = 4).

(F) mRNA levels of *Ucp1*, *Elovl3*, and *Cytc* in scramble (Scr) and siHSF1-immortalized beige adipocytes with ADV-mediated GFP or A2B1 overexpression upon transcriptional inhibition with actinomycin D at indicated time (n = 4).

(G) mRNA levels of *Hsf1* and *A2b1* in BAT and iWAT of NCD mice (n = 6).

(H) RIP assay assessing A2B1 binding on 3′UTR of *Pgc1α*, *Ucp1*, *Elovl3*, and *Cytc* in immortalized brown adipocytes (n = 3).

Statistical significance was assessed by unpaired Student's t test (A, G, and H). Data are presented as mean ± SEM and *p < 0.05 and **p < 0.01.